REVIEW OF THE SPACE MAPPING APPROACH
TO ENGINEERING OPTIMIZATION AND MODELING

M. H. Bakr, J. W. Bandler and K. Madsen

SOS-99-25-RR

(Revised August 2000)

REVIEW OF THE SPACE MAPPING APPROACH
TO ENGINEERING OPTIMIZATION AND MODELING

Mohamed H. Bakr, John W. Bandler and Kaj Madsen

Abstract   We review the Space Mapping (SM) concept and its applications in engineering optimization and modeling. The aim of SM is to avoid computationally expensive calculations encountered in simulating an engineering system. The existence of less accurate but fast physically-based models is exploited. SM drives the optimization iterates of the time-intensive model using the fast model. Several algorithms have been developed for SM optimization, including the original SM algorithm, Aggressive Space Mapping (ASM), Trust Region Aggressive Space Mapping (TRASM) and Hybrid Aggressive Space Mapping (HASM). An essential subproblem of any SM based optimization algorithm is parameter extraction. The uniqueness of this optimization subproblem has been crucial to the success of SM optimization. Different approaches to enhance the uniqueness are reviewed. We also discuss new developments in Space Mapping-based Modeling (SMM). These include Space Derivative Mapping (SDM), Generalized Space Mapping (GSM) and Space Mapping-based Neuromodeling (SMN). Finally, we address open points for research and future development.

M.H. Bakr and J.W. Bandler are with the Simulation Optimization Systems Research Laboratory and the Department of Electrical and Computer Engineering, McMaster University, Hamilton, Ontario, Canada, L8S 4K1.

J.W. Bandler is also with Bandler Corporation, P.O. Box 8083, Dundas, Ontario, Canada L9H 5E7.

K. Madsen is with the Department of Mathematical Modelling, Technical University of Denmark, DK-2800 Lyngby, Denmark.

I. INTRODUCTION

We review the Space Mapping (SM) [1-13] approach to engineering device and system optimization and modeling. The target of system optimization is to determine a set of values for the system parameters such that certain design specifications are satisfied. These specifications represent constraints on the system responses. Usually, a model of the physical system is utilized in simulating and thus optimizing the system.

Traditional optimization techniques [14-39] directly utilize the simulated system responses and possibly available derivatives. Engineering models used in simulating the system responses vary in accuracy and speed. Usually, accurate models are computationally expensive and less accurate models are fast. In some engineering problems, applying traditional optimization using the accurate models directly may be prohibitively impractical. On the other hand, applying optimization using the less accurate models may indicate feasibility of the design but could lead to unreliable results. These results must be validated using the accurate models or even using measurements. It follows that alternative optimization approaches are desirable.

SM establishes a mathematical link (mapping) between the spaces of the parameters of two different models of the same physical system. The accurate and time-intensive model is denoted as a "fine" model. The less accurate but fast model is denoted as a "coarse" model. For example, in the context of analog electrical circuit design, a fine model may be a time-intensive finite element solution of Maxwell equations while the coarse model may be a circuit-theoretic model with empirical algebraic formulas.

Clear distinction should be made between SM optimization and optimization using approximations such as polynomials, response surfaces or splines. All these methods establish a local approximation of the fine model responses using a set of fine model simulations. This approximation may be updated using new fine model points. On the other hand, SM exploits a coarse model that is physically based and capable of simulating the considered system for a wide range of parameter values. This physical model is not updated or changed during SM optimization.

All the SM-based optimization algorithms we will review utilize two steps. The first step optimizes the design parameters of the coarse model to satisfy the original design specifications. The second step establishes a mapping between the parameter spaces of the two models. The space-mapped design is then taken as the mapped image of the optimal coarse model design.

Parameter extraction is an important element in establishing the mapping. In this step, the coarse model parameters corresponding to a given fine model point are obtained. The extraction problem is essentially an optimization problem, and can lead to nonunique solutions.

The first SM-based optimization algorithm was introduced in [4]. This method assumes a linear mapping between the parameter spaces. This assumption may not be fulfilled if significant "misalignment" exists between the two spaces. Here, "misalignment" denotes the difference between the fine model response and the coarse model response for the same set of parameters. For two identical models there is no misalignment. The more the functional behaviours of the two models differ, the more the misalignment increases.

Aggressive Space Mapping (ASM) [5] eliminates the simulation overhead required in [4]. It exploits a quasi-Newton step in predicting the new iterates. The algorithm does not assume that the mapping is necessarily linear. However, the nonuniqueness of the parameter extraction step may lead to divergence or oscillations of the process [6].

Several approaches were suggested to improve the uniqueness of the extraction step in the ASM algorithm. These include Multi-Point Extraction (MPE) [6], the penalty approach [7] and the statistical parameter extraction approach [8]. The Aggressive Parameter Extraction (APE) algorithm [40] addresses the selection of perturbations utilized in the MPE process. APE classifies the possible solutions to the extraction problem. The perturbations are obtained by either solving a linear system of equations or through an eigenvalue problem.

Trust Region Aggressive Space Mapping (TRASM) [9, 10] integrates a trust region methodology with the ASM technique. It also exploits a Recursive Multi-Point Extraction (RMPE) procedure. The available information about the mapping between the two spaces is utilized in the RMPE.

Both ASM and TRASM assume the existence of a coarse model that has sufficient accuracy. In both algorithms coarse model simulations are used to guide the optimization iterates. If the coarse model is severely different from the fine model both algorithms are not likely to converge.

The Hybrid Aggressive Space Mapping (HASM) algorithm [11, 12] is designed to handle severely misaligned cases. The algorithm utilizes SM optimization as long as SM is converging. Otherwise, it switches to direct optimization.

The reviewed SM optimization algorithms actually automate and are consistent with traditional engineering practice. The rapid development of SM algorithms has not been accompanied, however, with corresponding theoretical development of convergence properties. A comprehensive theory has yet to be developed.

Several approaches have been proposed to utilize the SM concept in engineering modeling. SM-based modeling makes use of both the coarse model and the available mapping between the two spaces. We review three principal approaches: Space Derivative Mapping (SDM) [41], Generalized Space Mapping (GSM) [42] and Space Mapping-based Neuromodeling (SMN) [43, 44].

We start by reviewing some concepts and definitions relevant to engineering device and system optimization in Section II. The basic concept of SM optimization in discussed in Section III. The original SM optimization algorithm is discussed in Section IV. Section V addresses the ASM optimization algorithm along with two variant algorithms. Different approaches for improving the uniqueness of the parameter extraction procedure are also reviewed in Section V. TRASM and HASM are discussed in Sections VI and VII, respectively.

We also give a brief review of recent developments in SM-based modeling approaches in Section VIII. Open points of research in SM are discussed in Section IX. Finally, the conclusions are given in Section X.

II. SYSTEM OPTIMIZATION: SOME CONCEPTS AND DEFINITIONS

The physical system under consideration can be an electrical network, an electronic device, and so on. The performance of the system is described in terms of some measurable quantities. We denote these measurable quantities as the system response functions. The response functions are manipulated by adjusting certain designable parameters of the system. For example, the electrical response of a microstrip line can be adjusted by changing the physical width and length of the strip. Usually, some or all physical parameters are selected as designable parameters and thus can be optimized. We denote the vector of designable parameters by $\mathbf{x} \in \mathfrak{R}^n$.

Each response function relies on some other independent parameters, such as frequency, time and temperature [45]. We denote the ith response function by $R^i(\mathbf{x}, \xi_i)$, i=1, 2, …, N_R, where ξ_i is the vector of associated independent parameters.

The desired performance of the system is expressed by a set of specifications. These specifications represent constraints on the responses. They are functions of a set of the independent parameters. In practice, only a suitable discrete set of samples of the independent parameters is considered [45, 46]. Satisfying the specifications at these sampled values typically implies satisfying them for other values of the independent parameters.

Let μ_i be the number of discrete samples of the ith response. We define $\mathbf{R} \in \mathfrak{R}^m$ as the vector of sampled response functions. The kth component of $\mathbf{R}$ is given by

$$R_k = R^i(\mathbf{x}, \xi_i^j) \tag{1}$$

where $k = \sum_{p=1}^{i-1} \mu_p + j$ for $i = 1, 2, …, N_R$ and j=1, 2, …, μ_i. Here ξ_i^j is the jth sample of ξ_i and m is the total number of sampled response functions.

An error function defines the difference between the specification and the corresponding response. In some problems the specifications define a target response that should be reached. These types of specifications are denoted as single specifications [45]. In other problems, specifications define

6

upper and lower bounds on the respective response. For the case of single specifications the error functions are given by

$$e_k = w_k |R_k - S_k| \tag{2}$$

where S_k is the kth specification, $k \in K_s = \{k_1, k_2, \ldots, k_{N_c}\}$, the set of indices for the constrained responses, w_k is a nonnegative weight and N_c is the number of specifications.

In the case of upper and lower specifications, we classify the constraints on the response functions. We denote by S_{uk} and S_{lk} the kth upper and lower specification, respectively. Here, the error functions are given by

$$e_k = w_{uk}(R_k - S_{uk}), \quad k \in K_u \tag{3}$$

and

$$e_k = w_{lk}(S_{lk} - R_k), \quad k \in K_l \tag{4}$$

where K_u and K_l are sets of indices for the constrained responses and w_{uk} and w_{lk} are nonnegative weights. It is worth mentioning that simultaneous upper and lower specifications can be imposed on the same sampled response function, i.e., K_u and K_l may not be disjoint. Here $|K_u| + |K_l| = N_c$. Notice that the symbol $|\;|$ denotes the cardinality when applied to a set. Otherwise, it denotes the absolute value. We also denote by **e** the vector whose components are the error functions given by (2) or by (3) and (4).

It is clear from (3) and (4) that upper and lower specifications are meaningful only in the case of a real response while (2) is valid in general for complex responses. Also, a positive, negative or zero value of an error function indicates that the corresponding specification is violated, exceeded or just satisfied, respectively. A set of designable parameters for which **e** is nonpositive is denoted a feasible design. The set of all feasible designs defines a feasible region in the space of designable parameters. Fig. 1 illustrates the concepts of error functions, feasible design and feasible region.

The error vector **e** is evaluated for a given **x** using the vector of sampled responses **R**. **R** may be obtained by measuring the system responses. However, this approach is usually expensive and time consuming. Alternatively, **R** may be obtained by using a model of the physical system. This model

utilizes the knowledge available about the physical processes taking place within the system. Usually, different models exist for the same system. These models vary in their accuracy and the speed with which **R** is obtained. In the discussion that follows we assume that the system responses are obtained through simulation.

The problem of system design can be formulated as

$$\mathbf{x}^* = arg\left\{\min_{\mathbf{x}} U(\mathbf{x})\right\} \tag{5}$$

where $U(\mathbf{x})$ is a scalar objective function that is dependent on the error functions. $U(\mathbf{x})$ should offer a measure of the specifications' violation or satisfaction. A possible choice of $U(\mathbf{x})$ is the l_p norm [47], Huber norm [48, 49] or the generalized l_p function [38, 50]. The l_p norm of **e** is given by

$$\|\mathbf{e}\|_p = \left[\sum_{k=1}^{N_C} |e_k|^p\right]^{1/p} \tag{6}$$

The most commonly used norm is the l_2 norm, i.e., $p=2$. This norm is widely used because of its differentiability and its statistical properties. A large number of optimization techniques exist for least-squares optimization [22]. Solutions obtained using least-squares optimization can be altered significantly by the existence of a few wild data points.

Setting $p=1$ we have the l_1 norm

$$\|\mathbf{e}\|_1 = \sum_{k=1}^{N_C} |e_k| \tag{7}$$

This norm is robust to outliers. It finds wide application in data-fitting in the presence of gross errors [34], in analog fault location [51] and device modeling [37].

Setting $p=\infty$ we have the l_∞ norm

$$\|\mathbf{e}\|_\infty = \max_k |e_k| \tag{8}$$

which considers only the worst violated error function. Many system design problems can be formulated as a minimax optimization problem [25].

8

The l_1 and l_∞ norms are both nondifferentiable. Corresponding optimization algorithms tend to be more involved than least-squares algorithms. In general, the algorithms used to minimize the l_1 and l_∞ norms follow similar strategies. These algorithms solve the minimization problem in an iterative way. In [23, 24], the problem is formulated as a nonlinear program. Some methods utilize first-order derivatives of the error functions to construct sequential linearizations of the nonlinear program. Such methods are denoted as first-order methods. For example, in [32, 36] the linearization is used to construct a linear program that returns a suggested search direction. A line search is then executed in that direction. A trust region methodology [52] is integrated with the linear program formulation in [53]. Some of these first-order methods assure global convergence to a stationary point, for example [53]. However, they may yield a low convergence rate in the neighborhood of a solution if the problem is singular [54].

Another class of methods for the minimization of l_1 and l_∞ norms utilizes approximate second-order derivatives of the error functions. These methods solve the first-order optimality conditions using quasi-Newton methods [14, 19, 22]. They usually have a high convergence rate in the neighborhood of a solution. However, pure second-order methods do not guarantee global convergence. Hybrid methods [25, 34] combine both first-order and second-order methods. A first-order method is used far from the solution. Once the solution is approached, a switch to a second-order method is executed. Several switches can take place between the two methods.

Another norm that can be utilized as an objective function is the Huber norm [48, 49]. This norm is a hybrid combination between the l_1 and l_2 norms. It is defined by

$$\|\mathbf{e}\|_H = \sum_{k=1}^{N_c} \rho_\alpha(e_k) \tag{9}$$

where

$$\rho_\alpha(e_k) = \begin{cases} \dfrac{e_k^2}{2} & \text{if } |e_k| \le \alpha \\[2ex] \alpha|e_k| - \dfrac{e_k^2}{2} & \text{if } |e_k| > \alpha \end{cases} \tag{10}$$

where α is a threshold called the Huber threshold. This norm treats small errors in the l_2 sense while it treats large errors in the l_1 sense. Here, we adopt the engineering notation and use the word "norm" for the function (9) even though some of the basic norm properties are not satisfied. Huber optimization [39] is more robust against gross errors than least-squares optimization. It also offers less biased designs than those obtained using l_1 optimization [39].

The previously discussed norms, can be used to minimize the error functions towards zero. A design that corresponds to a zero error vector would be satisfactory if it were not for manufacturing tolerances. These tolerances are inevitable and may cause the constructed physical system to violate the specifications. It follows that optimization should continue to center the design within the feasible region [55-57]. The yield is defined as the percentage of the manufactured systems that satisfy the design constraints. Fig. 2 Illustrates the concepts of design centering and yield. Several algorithms have been developed with the aim of maximizing the yield [58-60].

The generalized l_p function [38, 50] was developed to enable optimization towards a better centered design. It makes use of the one-sided objective functions

$$H_p^+ = \left[\sum_k |e_k|^p \right]^{1/p}, \ \forall e_k \geq 0 \tag{11}$$

and

$$H_p^- = -\left[\sum_k (-e_k)^{-p} \right]^{-1/p}, \ \forall e_k < 0 \tag{12}$$

The generalized l_p function is equal to (11) if at least one of the specifications is violated. Otherwise, it is equal to (12).

We denote the optimization algorithms discussed thus far as 'direct optimization' algorithms. They utilize simulations of the optimized system and can be applied if the model simulation time is not extensive. Otherwise, direct optimization becomes prohibitive and alternative methods should be used. SM optimization was introduced as such an alternative.

III. SPACE MAPPING OPTIMIZATION: THE BASIC CONCEPT

We refer to the vectors of "fine" model parameters and corresponding "coarse" model parameters as $\mathbf{x}_f \in \mathfrak{R}^n$ and $\mathbf{x}_c \in \mathfrak{R}^n$, respectively. The optimal coarse model design $\mathbf{x}_c^*$ is obtained using only coarse model simulations. The corresponding response is denoted by $\mathbf{R}_c^*$. A minimax algorithm [25], if appropriate, may be used.

SM establishes a mathematical link (mapping) $\mathbf{P}$ between the two spaces [4]

$$\mathbf{x}_c = \mathbf{P}(\mathbf{x}_f) \tag{13}$$

such that

$$\left\| \mathbf{R}_f(\mathbf{x}_f) - \mathbf{R}_c(\mathbf{x}_c) \right\| \leq \varepsilon \tag{14}$$

The mapping $\mathbf{P}$ is valid over a region in the parameter space. An approximation to this mapping is established in an iterative way. We denote by $\mathbf{P}^{(j)}$ the available approximation to $\mathbf{P}$ at the jth iteration. The corresponding fine model design is given by

$$\mathbf{x}_f^{(j+1)} = \mathbf{P}^{(j)-1}(\mathbf{x}_c^*) \tag{15}$$

If it satisfies a certain termination criterion, it is accepted as the space mapped design $\bar{\mathbf{x}}_f$. Otherwise, the mapping is updated and a new design is calculated.

IV. THE ORIGINAL SM OPTIMIZATION ALGORITHM

At the jth iteration, the algorithm utilizes a set of fine model points $S_f^{(j)}$ defined by

$$S_f^{(j)} = \left\{ \mathbf{x}_f^{(1)}, \mathbf{x}_f^{(2)}, \ldots, \mathbf{x}_f^{(m_j)} \right\} \tag{16}$$

where $m_j = \left| S_f^{(j)} \right|$. The fine model response for every point in the set $S_f^{(j)}$ is simulated. A corresponding set of coarse model points $S_c^{(j)}$ defined by

$$S_c^{(j)} = \left\{ \mathbf{x}_c^{(1)}, \mathbf{x}_c^{(2)}, \ldots, \mathbf{x}_c^{(m_j)} \right\} \tag{17}$$

11

is then constructed. The points $\mathbf{x}_c^{(i)} \in S_c^{(j)}$, $i=1, 2, \ldots, m_j$ are obtained through the Single-Point Extraction (SPE) process (see Fig. 3)

$$\mathbf{x}_c^{(i)} = arg\left\{ \min_{\mathbf{x}_c} \left\| \mathbf{R}_f(\mathbf{x}_f^{(i)}) - \mathbf{R}_c(\mathbf{x}_c) \right\| \right\} \qquad (18)$$

$\mathbf{P}^{(j)}$ is then estimated using $S_f^{(j)}$ and $S_c^{(j)}$. Here, Every coarse model parameter is expressed as a linear combination of some predefined and fixed functions $\varphi_k(\mathbf{x}_f)$, $k=0, 1, \ldots, l$. It follows that

$$\mathbf{x}_c = \mathbf{P}^{(j)}(\mathbf{x}_f) = \mathbf{A}^{(j)}\boldsymbol{\varphi}(\mathbf{x}_f) \qquad (19)$$

where $\mathbf{A}^{(j)} \in \mathfrak{R}^{n\times(l+1)}$ is a matrix of constant coefficients and $\boldsymbol{\varphi}(\mathbf{x}_f)$ is given by

$$\boldsymbol{\varphi}(\mathbf{x}_f) = \begin{bmatrix} \varphi_0(\mathbf{x}_f) \\ \varphi_1(\mathbf{x}_f) \\ \vdots \\ \varphi_l(\mathbf{x}_f) \end{bmatrix} \qquad (20)$$

Relation (19) must be satisfied for every pair of corresponding points in $S_f^{(j)}$ and $S_c^{(j)}$. It follows that $\mathbf{A}^{(j)}$ should satisfy

$$\left[\mathbf{x}_c^{(1)} \ \mathbf{x}_c^{(2)} \cdots \mathbf{x}_c^{(m_j)} \right] = \mathbf{A}^{(j)} \left[\boldsymbol{\varphi}(\mathbf{x}_f^{(1)}) \ \boldsymbol{\varphi}(\mathbf{x}_f^{(2)}) \cdots \boldsymbol{\varphi}(\mathbf{x}_f^{(m_j)}) \right] \qquad (21)$$

In [4] it is assumed that the mapping between the two spaces is linear, i.e.,

$$\mathbf{x}_c = \mathbf{P}^{(j)}(\mathbf{x}_f) = \mathbf{B}^{(j)}\mathbf{x}_f + \mathbf{c}^{(j)} \qquad (22)$$

where $\mathbf{B}^{(j)} \in \mathfrak{R}^{n\times n}$ and $\mathbf{c}^{(j)} \in \mathfrak{R}^n$. The linear mapping (22) is equivalent to (19) with $\mathbf{A}^{(j)} = \left[\mathbf{c}^{(j)} \ \ \mathbf{B}^{(j)} \right]$ and $\varphi_k(\mathbf{x}_f) = x_{f,k}$, $k=1, 2, \ldots, n$, the kth component of the vector $\mathbf{x}_f$, $\varphi_0(\mathbf{x}_f) = 1$ and $l=n$. It follows that (21) can be written as

$$\left[\mathbf{x}_c^{(1)} \ \mathbf{x}_c^{(2)} \cdots \mathbf{x}_c^{(m_j)} \right] = \mathbf{A}^{(j)} \begin{bmatrix} 1 & 1 & \cdots & 1 \\ \mathbf{x}_f^{(1)} & \mathbf{x}_f^{(2)} & \cdots & \mathbf{x}_f^{(m_j)} \end{bmatrix} \qquad (23)$$

A least-squares solution for $\mathbf{A}^{(j)T}$ is thus given by

$$\mathbf{A}^{(j)T} = \left(\mathbf{D}^T\mathbf{D}\right)^{-1}\mathbf{D}^T\mathbf{Q} \tag{24}$$

where

$$\mathbf{D} = \begin{bmatrix} 1 & 1 & \dots & 1 \\ \mathbf{x}_f^{(1)} & \mathbf{x}_f^{(2)} & \dots & \mathbf{x}_f^{(m_j)} \end{bmatrix}^T \tag{25}$$

and

$$\mathbf{Q} = \left[\mathbf{x}_c^{(1)}\ \mathbf{x}_c^{(2)}\dots\mathbf{x}_c^{(m_j)}\right]^T \tag{26}$$

Once $\mathbf{A}^{(j)}$ is obtained, the suggested space-mapped design is

$$\mathbf{x}_f^{(m_j+1)} = \mathbf{P}^{(j)-1}(\mathbf{x}_c^*) = \mathbf{B}^{(j)-1}\left(\mathbf{x}_c^* - \mathbf{c}^{(j)}\right) \tag{27}$$

Here, the mapping is assumed to be one to one. The new point $\mathbf{x}_f^{(m_j+1)}$ is taken as an approximation to the

optimal fine model design $\mathbf{x}_f^*$ if the condition

$$\left\|\mathbf{R}_f(\mathbf{x}_f^{(m_j+1)}) - \mathbf{R}_c(\mathbf{x}_c^*)\right\| \le \varepsilon \tag{28}$$

is satisfied. In this case we take $\overline{\mathbf{x}}_f = \mathbf{x}_f^{(m_j+1)}$. Otherwise, the set $S_f^{(j)}$ is augmented by $\mathbf{x}_f^{(m_j+1)}$ and the set

$S_c^{(j)}$ is augmented by $\mathbf{x}_c^{(m_j+1)}$ obtained using (18). The algorithm steps using (23)-(28) are then repeated

using the augmented sets. Fig. 4 illustrates one iteration of the algorithm.

This algorithm is simple but it suffers from a number of drawbacks. First, to have the algorithm

started an initial set of fine model points $S_f^{(0)}$ must be created. The points in $S_f^{(0)}$ are selected in the

vicinity of a reasonable candidate for the fine model design. In [4] it is suggested to take $\mathbf{x}_f^{(1)} = \mathbf{x}_c^*$. The

other m_0-1 points are selected by perturbation with $m_0 \ge n+1$. Simulating $S_f^{(0)}$ represents a significant

overhead for the algorithm. The mapping is also assumed to be linear, which may not be true for

significantly misaligned models. Also, coarse model points are obtained through SPE. Nonuniqueness of

the extracted parameters may lead to an erroneous mapping estimation and divergence of the algorithm.

These drawbacks led to the development of the Aggressive Space Mapping (ASM) algorithm [5].

V. THE ASM ALGORITHM

The space-mapped design $\bar{\mathbf{x}}_f$ is a solution to the system of nonlinear equations

$$\mathbf{f} = \mathbf{P}(\mathbf{x}_f) - \mathbf{x}_c^* = \mathbf{0} \tag{29}$$

ASM solves (29) in an iterative manner. Let $\mathbf{x}_f^{(j)}$ be the jth iterate in the solution of (29). The next iterate $\mathbf{x}_f^{(j+1)}$ is found by a quasi-Newton iteration

$$\mathbf{x}_f^{(j+1)} = \mathbf{x}_f^{(j)} + \mathbf{h}^{(j)} \tag{30}$$

$\mathbf{h}^{(j)}$ is a solution of

$$\mathbf{B}^{(j)} \mathbf{h}^{(j)} = -\mathbf{f}^{(j)} \tag{31}$$

where $\mathbf{f}^{(j)} = \mathbf{P}^{(j)}(\mathbf{x}_f^{(j)}) - \mathbf{x}_c^*$. $\mathbf{B}^{(j)}$ is an approximation to the Jacobian $\mathbf{J}_m$ of $\mathbf{f}$ with respect to $\mathbf{x}_f$ at $\mathbf{x}_f^{(j)}$. $\mathbf{J}_m$ is defined by

$$\mathbf{J}_m(\mathbf{x}_f^{(j)}) = \left(\frac{\partial \mathbf{f}^T(\mathbf{x}_f)}{\partial \mathbf{x}_f} \right)^T_{\mathbf{x}_f = \mathbf{x}_f^{(j)}} \tag{32}$$

If the mapping between the two spaces is linear, similar to (22), the matrix $\mathbf{J}_m$ is constant. Otherwise, it is a function of the fine model parameters. The initial approximation to $\mathbf{J}_m$ is taken as $\mathbf{B}^{(0)} = \mathbf{I}$, the identity matrix. $\mathbf{B}^{(j)}$ is updated at each iteration using Broyden's rank one update [19]

$$\mathbf{B}^{(j+1)} = \mathbf{B}^{(j)} + \frac{\mathbf{f}^{(j+1)} - \mathbf{f}^{(j)} - \mathbf{B}^{(j)} \mathbf{h}^{(j)}}{\mathbf{h}^{(j)T} \mathbf{h}^{(j)}} \mathbf{h}^{(j)T} \tag{33}$$

The formula (33) can be simplified using (31) to

$$\mathbf{B}^{(j+1)} = \mathbf{B}^{(j)} + \frac{\mathbf{f}^{(j+1)}}{\mathbf{h}^{(j)T} \mathbf{h}^{(j)}} \mathbf{h}^{(j)T} \tag{34}$$

The error vector $\mathbf{f}^{(j)}$ is obtained by evaluating $\mathbf{P}^{(j)}(\mathbf{x}_f^{(j)})$, which is done indirectly through SPE. The algorithm terminates if $\left\| \mathbf{f}^{(j)} \right\|$ becomes sufficiently small. A complete iteration of the algorithm is shown in Fig. 5.

The ASM algorithm solves the problem of the overhead encountered in the initial stage of the original SM optimization algorithm. Also, while (23) assumes that the mapping is linear, ASM does not make this assumption. The output of the ASM algorithm is the space-mapped design $\overline{\mathbf{x}}_f$ and the matrix $\overline{\mathbf{B}}$, which approximates the Jacobian $\mathbf{J}_m$ at $\overline{\mathbf{x}}_f$. However, the nonuniqueness problem of the SPE process remains. An incorrect value for the vector $\mathbf{P}^{(j)}(\mathbf{x}_f^{(j)})$ may cause the algorithm to diverge or exhibit oscillatory behavior.

Two interesting, intuitive, variants of the ASM algorithm are suggested in [61, 62]. The basic idea of both algorithms is practically the same. The iterate is given by (31) with the matrix $\mathbf{B}^{(j)}$ fixed at $\mathbf{B}^{(j)} = \mathbf{I}$. Broyden's updating formula is not utilized. These "steepest-descent" approaches may succeed if the mapping between the two spaces is essentially represented by a shift.

An example of ASM optimization is the three-section microstrip impedance transformer [63]. The filter structure is shown in Fig. 6. The fine model utilizes a full-wave electromagnetic simulator (Sonnet's *em* [64]). The coarse model utilizes the empirical microstrip line and microstrip step models available in the circuit simulator OSA90/hope [65]. The designable parameters are the width and physical length of each microstrip line. Here, the reflection coefficient $|S_{11}|$ is used to match the two model responses. ASM terminated using only 9 fine model simulations. The initial and space-mapped responses are shown in Figs. 7 and 8, respectively. A frequency sweep of the fine model requires about one hour of CPU time on an HP workstation model 715/33. The coarse model simulation time is a fraction of a second. Optimizing this circuit using direct methods would have probably required dozens of fine model simulations.

Several approaches were suggested to enhance the uniqueness of the parameter extraction process. The first approach is Multi-Point Extraction (MPE) [6]. It simultaneously matches a number of points in both spaces. MPE aims at matching not only the function values but also the first-order derivatives. The point $\mathbf{x}_c^{(j+1)}$ corresponding to $\mathbf{x}_f^{(j+1)}$ is found by solving

$$\mathbf{x}_c^{(j+1)} = arg\left\{ \min_{\mathbf{x}_c} \; \left\| \; [\mathbf{e}_0^{\,T} \quad \mathbf{e}_1^{\,T} \quad \cdots \quad \mathbf{e}_{N_p}^{\,T}]^T \; \right\| \right\} \tag{35}$$

where

$$\mathbf{e}_0 = \mathbf{R}_c(\mathbf{x}_c) - \mathbf{R}_f(\mathbf{x}_f^{(j+1)}) \tag{36}$$

and

$$\mathbf{e}_i = \mathbf{R}_c(\mathbf{x}_c + \Delta\mathbf{x}_c^{(i)}) - \mathbf{R}_f(\mathbf{x}_f^{(j+1)} + \Delta\mathbf{x}_f^{(i)}), \; i{=}1, 2, \ldots, N_p \tag{37}$$

It follows that the set of utilized fine model points is $V = \left\{ \mathbf{x}_f^{(j+1)} \right\} \cup \left\{ \mathbf{x}_f^{(j+1)} + \Delta\mathbf{x}_f^{(i)} \mid i = 1, 2, \ldots, N_p \right\}$. The perturbations $\Delta\mathbf{x}_c^{(i)}$ and $\Delta\mathbf{x}_f^{(i)}$ are related by [6]

$$\Delta\mathbf{x}_c^{(i)} = \Delta\mathbf{x}_f^{(i)}, \; i{=}1, 2, \ldots, N_p \tag{38}$$

Integrating this MPE in the ASM algorithm faces some difficulty. The number of fine model points utilized is arbitrary and there is no clear way of how to select them. Also, available information about the mapping between the two spaces is not utilized. This MPE procedure is illustrated in Fig. 9.

Another approach is suggested in [7]. Here, the point $\mathbf{x}_c^{(j+1)}$ is obtained by solving the penalized SPE process

$$\mathbf{x}_c^{(j+1)} = arg\left\{ \min_{\mathbf{x}_c} \left(\left\| \mathbf{R}_f(\mathbf{x}_f^{(j+1)}) - \mathbf{R}_c(\mathbf{x}_c) \right\| + w \left\| \mathbf{x}_c - \mathbf{x}_c^* \right\| \right) \right\} \tag{39}$$

where w is a weighting factor. If the parameter extraction problem is not unique (39) is favored over (18). The solution of the extraction problem is biased towards the point $\mathbf{x}_c^*$ and thus drives the error vector $\mathbf{f}$ to zero as the algorithm proceeds. If w is too large the matching between the responses is poor. On the other

hand, too small a value of w makes the penalty term ineffective. In which case, the uniqueness of the extraction step may not be enhanced.

A statistical approach to parameter extraction is suggested in [8]. Here, the SPE process (18) is initiated from different starting points. The extraction process is unique if the same values of the extracted parameters are obtained for each starting point. Otherwise, the solution is nonunique. In this case, the solution that results in the best match in terms of some norm is selected.

In [8] it is suggested that a set of N_s starting points be randomly selected in a region $D \subset \Re^n$ where the solution $\mathbf{x}_c^{(j+1)}$ is expected. For the jth iteration, D is defined by

$$x_{c,i} \in \left[x_{c,i}^* - 2\left|f_i^{(j)}\right|, x_{c,i}^* + 2\left|f_i^{(j)}\right| \right] \tag{40}$$

for $i=1, 2, \ldots, n$. Fig. 10 illustrates the selection of the interval D for the two-dimensional case.

The Aggressive Parameter Extraction (APE) algorithm [40] addresses the selection of the perturbations utilized in the MPE process. It suggests perturbations that are likely to impact the uniqueness of the parameter extraction step.

APE classifies the possible solutions of the parameter extraction problem as either locally nonunique or locally unique. In the locally nonunique case the minimum of the extraction problem is assumed over a surface. For the locally unique case the minimum is assumed at a point. Figs. 11 and 12 illustrate the classification of the extracted parameters.

To illustrate the APE algorithm, assume that the point $\mathbf{x}_c^{(j+1)}$ corresponding to $\mathbf{x}_f^{(j+1)}$ is obtained through MPE. The utilized set of fine model points is V with $|V| = N$. If $\mathbf{x}_c^{(j+1)}$ is locally nonunique, APE suggests a new point to be added to V. This point is likely to make the extracted parameters using the augmented set locally unique. It is obtained by solving a linear system of equations that utilizes the gradients and Hessians of coarse model responses at $\mathbf{x}_c^{(j+1)}$.

If $\mathbf{x}_c^{(j+1)}$ is locally unique, the new point $\mathbf{x}_f^{(N)}$ to be added to the set V is obtained by solving the eigenvalue problem

$$\left(\mathbf{J}_c(\mathbf{x}_c^{(j+1)})^T \mathbf{J}_c(\mathbf{x}_c^{(j+1)}) + \mathbf{I}\right)\Delta\mathbf{x}_c^{(N)} = \lambda\Delta\mathbf{x}_c^{(N)} \tag{41}$$

and

$$\mathbf{x}_f^{(N)} = \mathbf{x}_f^{(j+1)} + \Delta\mathbf{x}_f^{(N)} \tag{42}$$

where $\mathbf{J}_c$ is the Jacobian of coarse model responses. Here, the coarse model perturbation $\Delta\mathbf{x}_c^{(N)}$ and the fine model perturbation $\Delta\mathbf{x}_f^{(N)}$ are related by the available mapping. The obtained perturbation is scaled to satisfy a certain trust region.

VI. THE TRASM ALGORITHM

TRASM [9, 10] integrates a trust region methodology [52] with the ASM technique. Similar to ASM, TRASM aims at solving (29). However, instead of utilizing a quasi-Newton step the problem is solved as a least-squares problem. In the jth iteration the objective of TRASM is to minimize $\left\|\mathbf{f}^{(j+1)}\right\|_2^2$ within a certain trust region. To achieve this, TRASM utilizes a linearization of the vector function $\mathbf{f}^{(j+1)}$. The linearized objective function is thus given by

$$L(\mathbf{x}^{(j)}, \mathbf{h}^{(j)}) = \left\|\mathbf{f}^{(j)} + \mathbf{B}^{(j)}\mathbf{h}^{(j)}\right\|_2^2 \tag{43}$$

The suggested step is obtained by solving

$$\mathbf{h}^{(j)} = arg\left\{\min_{\mathbf{h}} \ \left\|\mathbf{f}^{(j)} + \mathbf{B}^{(j)}\mathbf{h}\right\|_2^2\right\} \tag{44}$$

$$\text{subject to } \left\|\mathbf{h}^{(j)}\right\|_2 \le \delta^{(j)} \tag{45}$$

where $\delta^{(j)}$ is the size of the trust region. The solution of (43)-(45) is obtained by solving [66, 67]

$$(\mathbf{B}^{(j)T}\mathbf{B}^{(j)} + \lambda^{(j)}\mathbf{I})\mathbf{h}^{(j)} = -\mathbf{B}^{(j)T}\mathbf{f}^{(j)} \tag{46}$$

where $\lambda^{(j)}$ correlates to $\delta^{(j)}$. The larger the value of $\delta^{(j)}$ the smaller the value of $\lambda^{(j)}$ and vice versa. TRASM makes use of the algorithm suggested in [68] to determine the value of $\lambda^{(j)}$.

The suggested iterate is $\mathbf{x}_f^{(j+1)} = \mathbf{x}_f^{(j)} + \mathbf{h}^{(j)}$. Unlike ASM, $\mathbf{x}_f^{(j+1)}$ is accepted only if it satisfies a success criterion with respect to the reduction in the ℓ_2 norm of the vector $\mathbf{f}$. The success criterion utilized by TRASM is

$$\frac{\left(\left\|\mathbf{f}^{(j)}\right\| - \left\|\mathbf{f}_k^{(j+1)}\right\|\right)}{\left(\left\|\mathbf{f}^{(j)}\right\| - \left\|\mathbf{f}^{(j)} + \mathbf{B}^{(j)}\,\mathbf{h}^{(j)}\right\|\right)} > 0.01 \tag{47}$$

The subscript k indicates the number of points utilized in the Recursive Multi-Point Extraction (RMPE). It follows that $k = |V|$, where V is the set of fine model points used in the RMPE. Initially $V = \left\{\mathbf{x}_f^{(j+1)}\right\}$ and $k=1$.

If (47) is satisfied $\mathbf{x}_f^{(j+1)}$ is accepted and $\mathbf{B}^{(j)}$ is updated using (33). Otherwise, the validity of the extraction process leading to $\mathbf{f}_k^{(j+1)}$ is suspect. The residual vector $\mathbf{f}_k^{(j+1)}$ is then used to construct a temporary point $\mathbf{x}_t^{(k)}$ from the point $\mathbf{x}_f^{(j+1)}$ by using (46). The set V is updated to $V \cup \mathbf{x}_t^{(k)}$. RMPE is then repeated using the augmented set V to get $\mathbf{f}_{k+1}^{(j+1)}$. RMPE is given by (35)-(37) with (38) replaced by

$$\Delta\mathbf{x}_c^{(i)} = \mathbf{B}^{(j)}\,\Delta\mathbf{x}_f^{(i)} \tag{48}$$

Thus, the available information about the mapping between the two spaces is exploited. Fig. 13 illustrates the RMPE procedure.

The new error vector $\mathbf{f}_{k+1}^{(j+1)}$ either satisfies (47) or it is used to obtain another additional point which is then added to the set V. RMPE is then repeated until the extracted parameters are trusted (see Fig. 14).

TRASM trusts the vector of extracted parameters if it approaches a limit. The sufficient condition for this is

$$\left\|\mathbf{f}_{k+1}^{(j+1)} - \mathbf{f}_k^{(j+1)}\right\| \le \varepsilon \tag{49}$$

19

The trusted value of $\mathbf{f}_k^{(j+1)}$ is denoted simply by $\mathbf{f}^{(j+1)}$. If $\mathbf{f}^{(j+1)}$ satisfies (47), $\mathbf{x}_f^{(j+1)}$ is accepted and the matrix $\mathbf{B}^{(j)}$ is updated using (33). Otherwise, the accuracy of the linearization used to predict $\mathbf{h}^{(j)}$ is suspected. Thus, to ensure a successful step from the current point $\mathbf{x}_f^{(j)}$, the trust region size is shrunk and a new suggested point $\mathbf{x}_f^{(j+1)}$ is obtained. During RMPE we may have $|V| = n+1$. In this case, sufficient information is available to obtain an estimate for the Jacobian $\mathbf{J}_f^{(j)}$ of the fine model responses. $\mathbf{J}_f^{(j)}$ is then used to obtain an alternative $\mathbf{h}^{(j)}$.

The size of the trust region is updated at the end of each iteration based on the match between the actual reduction and the predicted reduction in $\|\mathbf{f}\|$. The trust region size is increased if the condition

$$\left(\left\| \mathbf{f}^{(j)} \right\| - \left\| \mathbf{f}^{(j+1)} \right\| \right) \geq 0.80 \left(\left\| \mathbf{f}^{(j)} \right\| - \left\| \mathbf{f}^{(j)} + \mathbf{B}^{(j)} \, \mathbf{h}^{(j)} \right\| \right) \tag{50}$$

is satisfied. It should be mentioned that the constants utilized in (47) and (50) are arbitrary.

The design of a High-Temperature Superconducting (HTS) filter [1] is carried out using TRASM [9]. The filter is shown in Fig. 15. The designable parameters are L_1, L_2, L_3, S_1, S_2 and S_3. The coarse model exploits the empirical models of a microstrip line, coupled lines and open stubs available in OSA90/hope. The fine model employs the method of moments simulator *em*. The initial fine model response is shown in Fig. 16. Only 8 fine model simulations were required by TRASM. The space-mapped response is shown in Fig. 17. On a Sun SPARCstation 10, the fine model requires one hour of CPU time per frequency point. The coarse model requires a fraction of a second for a complete sweep.

Both the ASM and TRASM algorithms are efficient. The number of required fine model simulations is of the order of the problem dimensionality. However, both models depend on the existence of a coarse model that is fast and has sufficient accuracy. The main prediction steps in (31) and (46) show that coarse model simulations are used to guide the optimization iterates. If the coarse model is severely different from the fine model the ASM algorithm is likely to diverge and TRASM may stop at a solution that is not close to the required design. To overcome this problem the Hybrid Aggressive Space Mapping (HASM) algorithm was developed.

VII. THE HASM ALGORITHM

HASM exploits SM when effective, otherwise it defaults to direct optimization. Two objective functions are utilized by the algorithm. The first objective function is

$$\left\| \mathbf{f}^{(j)} \right\|_2^2 = \left\| \mathbf{P}^{(j)}(\mathbf{x}_f^{(j)}) - \mathbf{x}_c^* \right\|_2^2 \tag{51}$$

which is the TRASM objective function. The second objective function is

$$\left\| \mathbf{g}^{(j)} \right\|_2^2 = \left\| \mathbf{R}_f(\mathbf{x}_f^{(j)}) - \mathbf{R}_c(\mathbf{x}_c^*) \right\|_2^2 \tag{52}$$

and is denoted as the direct optimization objective function.

HASM consists of two phases: the first phase follows the TRASM strategy while the second phase exploits direct optimization. For switching between the two phases the algorithm utilizes a relationship that relates the established mapping to the first-order derivatives of both models [11, 12]. This relationship stipulates that if $\mathbf{x}_c$ corresponds to $\mathbf{x}_f$ through a parameter extraction process, then the Jacobian $\mathbf{J}_f$ of the fine model response at $\mathbf{x}_f$ and the Jacobian $\mathbf{J}_c$ of the coarse model response at $\mathbf{x}_c$ are related by

$$\mathbf{J}_f = \mathbf{J}_c \, \mathbf{B} \tag{53}$$

where $\mathbf{B}$ is a valid mapping between the two spaces at $\mathbf{x}_c$ and $\mathbf{x}_f$. Another important relationship that follows from (53) is

$$\mathbf{B} = \left(\mathbf{J}_c^T \mathbf{J}_c\right)^{-1} \mathbf{J}_c^T \mathbf{J}_f \tag{54}$$

(54) assumes that $\mathbf{J}_c$ is full rank and $m \geq n$, where m is the dimensionality of both $\mathbf{R}_f$ and $\mathbf{R}_c$.

In the jth iteration we assume the existence of a trusted $\mathbf{x}_c^{(j)} = \mathbf{P}^{(j)}(\mathbf{x}_f^{(j)})$. The step taken is given by (46) where $\mathbf{x}_f^{(j+1)} = \mathbf{x}_f^{(j)} + \mathbf{h}^{(j)}$. SPE is then applied at $\mathbf{x}_f^{(j+1)}$ to get $\mathbf{f}_1^{(j+1)} = \mathbf{P}(\mathbf{x}_f^{(j+1)}) - \mathbf{x}_c^*$.

The first phase utilizes two success criteria related to the reduction in (51) and (52). The first success criterion is given by (47). The success criterion related to (52) is given by

$$\left\| \mathbf{g}^{(j+1)} \right\| < \left\| \mathbf{g}^{(j)} \right\| \tag{55}$$

$\mathbf{x}_f^{(j+1)}$ is accepted if (55) is satisfied. The first phase continues and the matrix $\mathbf{B}^{(j)}$ is updated if (47) is also satisfied for a trusted $\mathbf{f}^{(j+1)}$.

Switching to the second phase takes place in two cases. The first case occurs if (55) is not satisfied. The second phase is then supplied by $\mathbf{x}_f^{(j)}$, $\mathbf{J}_f^{(j)}$ and $\mathbf{f}^{(j)}$. Here, $\mathbf{J}_f^{(j)}$ is estimated from $\mathbf{J}_c^{(j)}$ and $\mathbf{B}^{(j)}$ by using (53).

The second case occurs when $\mathbf{x}_f^{(j+1)}$ satisfies (55) but does not satisfy (47) for a trusted $\mathbf{f}^{(j+1)}$. $\mathbf{B}^{(j)}$ is updated to $\mathbf{B}^{(j+1)}$ using (33). The second phase is supplied with $\mathbf{x}_f^{(j+1)}$, $\mathbf{f}^{(j+1)}$ and $\mathbf{J}_f^{(j+1)}$. $\mathbf{J}_f^{(j+1)}$ is estimated from $\mathbf{J}_c^{(j+1)}$ and $\mathbf{B}^{(j+1)}$ by using (53). If $|V|$ reaches $n+1$ during RMPE, $\mathbf{J}_f^{(j+1)}$ is instead estimated through finite differences.

The second phase utilizes the first-order derivatives supplied by the first phase to carry out a number of successful iterations with the target of minimizing (52). At the end of each successful iteration parameter extraction is applied at the new iterate $\mathbf{x}_f^{(k+1)}$ and is used to check whether a switch to the first phase is possible. Here, k is used as an index for the iterations of the second phase. In the original implementation, switching back to the first phase takes place if

$$\left\| \mathbf{f}^{(k+1)} \right\| < \left\| \mathbf{f}^{(k)} \right\| \tag{56}$$

In this case $\mathbf{J}_c^{(k+1)}$ is evaluated at $\mathbf{x}_c^{(k+1)} = \mathbf{P}(\mathbf{x}_c^{(k+1)})$. $\boldsymbol{B}$ is then recovered using (54). Fig. 18 illustrates the connection between SM optimization and direct optimization.

HASM is illustrated by considering a six-section H-plane waveguide filter [69, 70]. The filter is shown in Fig. 19. The fine model utilizes the finite element simulator HP HFSS [71] through HP Empipe3D [72]. The designable parameters are the four septa widths W_1, W_2, W_3 and W_4 and the three waveguide-section lengths L_1, L_2 and L_3. The coarse model consists of lumped inductances and dispersive transmission line sections. It is simulated using OSA90/hope. A simplified version of a formula due to Marcuvitz [73] is utilized in evaluating the inductances. The coarse model is shown in Fig. 20. The responses obtained through different design stages are shown in Figs. 21 and 22.

In a later implementation, both the recovery of **B** and the switching back criterion were modified. The mapping recovery step (54) is made better conditioned by constraining **B** to be close to the identity matrix **I**. This follows from the fact that the fine and coarse models share the same physical background [42]. **B** is thus obtained by solving

$$\mathbf{B} = arg\left\{ \min_{\mathbf{B}} \left\| \; [\; \mathbf{e}_1^T \; \mathbf{e}_2^T \cdots \mathbf{e}_n^T \; \; w\Delta\mathbf{b}_1^T \; w\Delta\mathbf{b}_2^T \cdots w\,\Delta\mathbf{b}_n^T \;]^T \; \right\|_2^2 \right\} \tag{57}$$

where $\mathbf{e}_i$ is the ith column of the matrix

$$\mathbf{E}^{(k+1)} = \mathbf{J}_f^{(k+1)} - \mathbf{J}_c^{(k+1)} \mathbf{B} \tag{58}$$

$\Delta\mathbf{b}_i$ is the ith column of the matrix

$$\Delta\mathbf{B} = \mathbf{B} - \mathbf{I} \tag{59}$$

The solution to (57) is given by

$$\mathbf{B} = \left(\mathbf{J}_c^{(k+1)T} \mathbf{J}_c^{(k+1)} + w^2\mathbf{I} \right)^{-1} \left(\mathbf{J}_c^{(k+1)T} \mathbf{J}_f^{(k+1)} + w^2\mathbf{I} \right) \tag{60}$$

(60) is identical to (54) if w=0. In this modified implementation switching back to the first phase takes place if **B** given by (60) is able to predict with sufficient accuracy the reduction in $\left\| \mathbf{f}^{(k)} \right\|$.

23

VIII. SM-BASED MODELING

Thus far we focused on optimization algorithms. In this section we briefly discuss some of the SM-based modeling algorithms. The basic concept is to establish a mapping between the parameter spaces that is given by (13) and (14). The fine model response is then approximated by

$$\mathbf{R}_f(\mathbf{x}_f) \approx \mathbf{R}_c(\mathbf{P}(\mathbf{x}_f)) \tag{61}$$

The model given by (61) offers a fast approximation to the time-intensive fine model response. SM-based modeling approaches differ in the way in which the mapping is established, the nature of the mapping and the region of validity of the obtained model. We review three of these algorithms; Space Derivative Mapping (SDM), Generalized Space Mapping (GSM) and Space Mapping-based Neuromodeling (SMN). Fig. 23 illustrates the concept of SM based modeling.

Space Derivative Mapping (SDM) [41]

This algorithm develops a locally valid approximation of the fine model in the vicinity of a particular point $\overline{\mathbf{x}}_f$. We denote by $\overline{\mathbf{J}}_f$ the Jacobian of the fine model responses at $\overline{\mathbf{x}}_f$. The first step of the algorithm is to obtain the point $\overline{\mathbf{x}}_c$ corresponding to $\overline{\mathbf{x}}_f$ through the SPE problem (18). The Jacobian $\overline{\mathbf{J}}_c$ at $\overline{\mathbf{x}}_c$ may be estimated by finite differences. Both (18) and the evaluation of $\overline{\mathbf{J}}_c$ should add no significant overhead. The mapping matrix $\mathbf{B}$ is then calculated by applying (54) as

$$\mathbf{B} = \left(\overline{\mathbf{J}}_c^T \overline{\mathbf{J}}_c\right)^{-1} \overline{\mathbf{J}}_c^T \overline{\mathbf{J}}_f \tag{62}$$

Once $\mathbf{B}$ is available the linear mapping is given by

$$\mathbf{x}_c = \mathbf{P}(\mathbf{x}_f) = \overline{\mathbf{x}}_c + \mathbf{B}(\mathbf{x}_f - \overline{\mathbf{x}}_f) \tag{63}$$

The SDM model is given by (61) with $\mathbf{P}$ given by (63). In a later implementation, the matrix $\mathbf{B}$ is estimated using (60).

Generalized Space Mapping (GSM) Modeling [42]

This approach integrates three previously suggested SM modeling concepts [4, 5, 74]. The model is expected to be accurate in a region of the fine model space $D \subset \mathfrak{R}^n$. The mapping between the two spaces is assumed to be of the form

$$\mathbf{x}_c = \mathbf{P}(\mathbf{x}_f) = \mathbf{B}\,\mathbf{x}_f + \mathbf{c} \tag{64}$$

A set of fine model points $V \subset D$ is constructed. The mapping parameters $\mathbf{B}$ and $\mathbf{c}$ are then obtained through the optimization procedure

$$[\mathbf{B}, \mathbf{c}] = arg\left\{ \min_{\mathbf{B},\,\mathbf{c}} \; \left\| \; [\mathbf{e}_1^{\,T} \quad \mathbf{e}_2^{\,T} \quad \cdots \quad \mathbf{e}_N^{\,T}]^T \; \right\| \right\} \tag{65}$$

where

$$\mathbf{e}_i = \mathbf{R}_c(\mathbf{B}\,\mathbf{x}_f^{(i)} + \mathbf{c}) - \mathbf{R}_f(\mathbf{x}_f^{(i)}) \tag{66}$$

where $\mathbf{x}_f^{(i)} \in V$, $i=1, 2, \ldots, N$ and $|V| = N$. A star-like set of points is utilized in [42]. This selection of V is illustrated in Fig. 24 for the three-dimensional case. In (65) $\mathbf{B}$ can be constrained to be close to $\mathbf{I}$ similar to (60).

Another variation of (65) that is pertinent to analog electrical circuit device modeling is to include the frequency as a mapped parameter. This is essential if there are constraints on the possible simulated frequencies of the coarse model [43]. Also, it is reported that the accuracy of the SM model is significantly improved by utilizing a frequency-sensitive mapping.

Space Mapping-based Neuromodeling (SMN) [43, 44]

In Section IV we noticed that the basic idea of the original SM optimization algorithm is to express each coarse model parameter as the sum of predefined functions of the fine model parameters. Relation (19) can be written as

$$x_{c,i} = \sum_{j=1}^{n} a_{ij}\,\varphi_j(\mathbf{x}_f) \tag{67}$$

25

Consider a three-layer Artificial Neural Network (ANN) [75]. The inputs to this network are the fine model parameters and the outputs approximate the corresponding coarse model parameters. It follows that each output can be expressed as (see Fig. 25)

$$y_i = \sum_{j=1}^{nh} a_{ij} \psi_j (\mathbf{w}_j^T \mathbf{x}_f + \theta_j) \tag{68}$$

where n_h is the number of hidden neurons and ψ_j is the activation function associated with the jth hidden neuron. Here, $\mathbf{a}_i = \begin{bmatrix} a_{i1} & a_{i2} & \cdots & a_{inh} \end{bmatrix}^T$ is the vector of weights associated with the ith output neuron, $\mathbf{w}_j$ is the vector of weights associated with the jth hidden neuron and θ_j is the corresponding threshold.

By comparing (67) and (68) we see that a trained ANN can approximate the mapping between the two spaces. The universal approximation theorem [75] assures that a three-layer ANN is capable of approximating any nonlinear mapping between the two spaces.

Similar to GSM, an ANN is trained to approximate the mapping between the two spaces in a subset D of the parameter space. Given a set of training points $V \subset D$, the training problem is given by

$$[\mathbf{W}, \boldsymbol{\theta}, \mathbf{A}] = arg \left\{ \min_{\mathbf{W}, \boldsymbol{\theta}, \mathbf{A}} \left\| \begin{bmatrix} \mathbf{e}_1^T & \mathbf{e}_2^T & \cdots & \mathbf{e}_N^T \end{bmatrix}^T \right\| \right\} \tag{69}$$

where

$$\mathbf{e}_i = \mathbf{R}_c(\mathbf{y}) - \mathbf{R}_f(\mathbf{x}_f^{(i)}) \tag{70}$$

and $i=1, 2, \ldots, N$ and $|V| = N$.

The optimized mapping parameters are defined by

$$\mathbf{W} = \begin{bmatrix} \mathbf{w}_1 & \mathbf{w}_2 & \cdots & \mathbf{w}_{nh} \end{bmatrix}, \ \boldsymbol{\theta} = \begin{bmatrix} \theta_1 & \theta_2 & \cdots & \theta_{nh} \end{bmatrix}^T \text{and } \mathbf{A} = \begin{bmatrix} \mathbf{a}_1 & \mathbf{a}_2 & \cdots & \mathbf{a}_n \end{bmatrix} \tag{71}$$

This approach is superior to other modeling approaches that utilize ANNs [76, 77] because it results in a simple neural network and utilizes fewer training points [43].

Several variations to this approach that are more pertinent to analog electrical circuit modeling have been suggested in [43, 44]. The main concept in all these variations is to obtain a frequency-

sensitive mapping that improves the accuracy of the SM model. The star distribution shown in Fig. 24 is also used for V. The GSM approach can be visualized as a special case of SMN where the ANN has only two layers with no hidden neurons (see Fig. 26).

IX. FUTURE RESEARCH IN SM

Coarse Model Generation

All the SM-based algorithms thus far depend on the existence of a coarse model with sufficient accuracy. The generation of such a model requires knowledge of the problem and is still the user's responsibility. We expect more research on the automated generation of fast coarse models that have sufficient accuracy. Lightly trained neural networks may be one possible solution to this problem.

Neural Network-Based SM Optimization

Recently, an SM neuromodeling approach was introduced [43, 44]. A pioneering work [78] extends this concept to SM optimization. Here, a SM Neuromodel is utilized in optimizing the fine model. The complexity of the ANN is increased in every iteration with the newly generated fine model points. We expect further research to be carried out in this direction.

Optimality Conditions of SM Optimization

Research is being carried out to develop a comprehensive theory for the optimality conditions of SM. Development of such a theory will help robustize the SM-based optimization algorithms.

Using Surrogate Models

Research is currently conducted on the integration of surrogate models [79-83] with SM optimization. Surrogate-based optimization aims at efficiently optimizing a computationally-expensive model. Unlike SM optimization, the design problem is not formulated as an equivalent nonlinear system. Alternatively, the original design problem is solved using an approximate model. This approximate model may be a less accurate physically-based model or an algebraic model. The generated iterates are

validated through fine model simulations. The accuracy of the surrogate model is improved in every iteration using the generated simulations. A novel work [84] combines SM and surrogate model optimization in a powerful algorithm. We expect that more research will be conducted in this area.

X. CONCLUSIONS

In this work we reviewed the SM approaches to engineering optimization and modeling. SM optimization makes use of the existence of a less accurate but fast model to accelerate the optimization problem. The algorithms reviewed include the original SM optimization algorithm, ASM, TRASM and HASM algorithms. The original SM optimization algorithm utilizes two corresponding sets of points to establish the mapping between the two spaces. ASM eliminates the overhead simulations to obtain the initial mapping. However, it suffers from the nonuniqueness of the parameter extraction subproblem. The TRASM algorithm integrates a trust region methodology with the ASM technique. It also utilizes a recursive multi-point extraction approach. HASM addresses the problem of severely misaligned coarse models. It allows switching between SM optimization and direct optimization. We also reviewed the different approaches for improving the uniqueness of the parameter extraction problem. These include multi-point extraction, penalized parameter extraction, statistical parameter extraction and aggressive parameter extraction. The different approaches for SM-based engineering modeling were briefly discussed. We reviewed the SDM, the GSM and the SMN algorithms. Finally, we suggested some of the open points for research in SM.

REFERENCES

[1]   J.W. Bandler, R.M. Biernacki, S.H. Chen, W.J. Gestinger, P.A. Grobelny, C. Moskowitz and S.H. Talisa, "Electromagnetic design of high-temperature superconducting filters," Int. J. Microwave and Millimeter-Wave Computer-Aided Engineering, vol. 5, pp. 331-343, 1995.

[2]   J.W. Bandler, R.M. Biernacki, S.H. Chen, P.A. Grobelny, C. Moskowitz and S.H. Talisa, "Electromagnetic design of high-temperature superconducting filters," IEEE MTT-S Int. Microwave Symp. Dig. (San Diego, CA), pp. 993-996, 1994.

[3]   J.W. Bandler, R.M. Biernacki, S.H. Chen, P.A. Grobelny and R.H. Hemmers, "Exploitation of coarse grid for electromagnetic optimization," IEEE MTT-S Int. Microwave Symp. Dig. (San Diego, CA), pp.381-384, 1994.

[4]   J.W. Bandler, R.M. Biernacki, S.H. Chen, P.A. Grobelny and R.H. Hemmers, "Space mapping technique for electromagnetic optimization," IEEE Trans. Microwave Theory Tech., vol. 42, pp. 2536-2544, 1994.

[5]   J.W. Bandler, R.M. Biernacki, S.H. Chen, R.H. Hemmers and K. Madsen, "Electromagnetic optimization exploiting aggressive space mapping," IEEE Trans. Microwave Theory Tech., vol. 43, pp. 2874-2882, 1995.

[6]   J.W. Bandler, R.M. Biernacki and S.H. Chen, "Fully automated space mapping optimization of 3D structures," IEEE MTT-S Int. Microwave Symp. Dig. (San Francisco, CA), pp. 753-756, 1996.

[7]   J.W. Bandler, R.M. Biernacki, S.H. Chen and Y.F. Huang, "Design optimization of interdigital filters using aggressive space mapping and decomposition," IEEE Trans. Microwave Theory Tech., vol. 45, pp. 761-769, 1997.

[8]   J.W. Bandler, R.M. Biernacki, S.H. Chen and D. Omeragić, "Space mapping optimization of waveguide filters using finite element and mode-matching electromagnetic simulators," IEEE MTT-S Int. Microwave Symp. (Denver, CO), pp. 635-638, 1997.

[9]   M.H. Bakr, J.W. Bandler, R.M. Biernacki, S.H. Chen and K. Madsen, "A trust region aggressive space mapping algorithm for EM optimization," IEEE Trans. Microwave Theory Tech., vol. 46, pp. 2412-2425, 1998.

[10]   J.W. Bandler, M.H. Bakr, N. Georgieva, M.A. Ismail and D.G. Swanson., Jr., "Recent results in electromagnetic optimization of microwave components, including microstrip T-junctions," Proc. 15th Annual Review of Progress in Applied Computational Electromagnetics ACES 99 (Monterey, CA), pp. 326-333, 1999.

[11]   M.H. Bakr, J.W. Bandler, N. Georgieva and K. Madsen, "A hybrid aggressive space mapping algorithm for EM optimization," IEEE Trans. Microwave Theory Tech., vol. 47, 1999.

[12]   J.W. Bandler, M.H. Bakr and J.E. Rayas-Sánchez, "Accelerated optimization of mixed EM/circuit structures," Proc. Workshop on Advances in Mixed Electromagnetic Field and Circuit Simulation, IEEE MTT-S Int. Microwave Symp. (Anaheim, CA), 1999.

[13]   J.W. Bandler and K. Madsen, "Space mapping for optimal engineering design," 19th IFIP TC7 Conference on System Modelling and Optimization Abstracts (Cambridge, UK), p. 34, 1999.

[14]   J.E. Dennis, Jr., and J.J. Moré, "Quasi-Newton methods, motivation and theory," SIAM Rev., vol. 19, pp. 46-89, 1977.

[15]   C.G. Broyden, "Quasi-Newton methods and their application to function minimization," Math. Comp., vol. 21, pp. 368-381, 1967.

[16]   W.C. Davidon, "Variable metric method for minimization," Rep. ANL-5900 Rev., Argonne National Laboratories, Argonne, IL, 1959

[17]   R. Fletcher and M.J.D. Powell, "A rapidly convergent descent method for minimization," Comput. J., vol. 6, pp. 163-168, 1963.

[18]   P.E. Gill and W. Murray, "Quasi-Newton methods for unconstrained minimzation," J. Inst. Math. Appl., vol. 9, pp. 91-108, 1972.

[19]   C.G. Broyden, "A class of methods for solving nonlinear simultaneous equations," Math. Comp., vol. 19, pp. 577-593, 1965.

[20]   R. Flectcher and C.M. Reeves, "Function minimisation by conjugate gradients," Comput. J., vol. 7, pp. 149-154, 1964.

[21]   D. Le, "A fast and robust unconstrained optimization method requiring minimum storage," Math. Program., vol. 32, pp. 41-68, 1985.

[22]   J.E. Dennis, Jr., and R.B. Schnabel, Numerical Methods for Unconstrained Optimization and Nonlinear Equations, Prentice-Hall, New Jersey, 1983.

[23]   A.D. Waren, L.S. Lasdon and D.F. Suchman, "Optimization in engineering design," Proc. IEEE, vol. 55, pp. 1885-1897, 1967.

[24]   W. Murray and M.L. Overton, "A projected Lagrangian algorithm for nonlinear ℓ_1 optimization," SIAM J. Scient. Stat. Comp., vol. 2, pp. 207-224, 1981.

[25]   J.W. Bandler, W. Kellermann and K. Madsen, "A superlinearly convergent minimax algorithm for microwave circuit design," IEEE Trans. Microwave Theory Tech., vol. MTT-33, pp. 1519-1530, 1985.

[26]   D. Angew, "Improved minimax optimization for circuit design," IEEE Trans. Circuits Syst., vol. CAS-28, pp. 791-803, 1981.

[27]   J.W. Bandler, S.H. Chen, S. Daijavad, W. Kellermann, M. Renault and Q.J. Zhang, "Large scale minimax optimization of microwave multiplexers," Proc. European Microwave Conf. (Dublin, Ireland), pp. 435-440, 1986.

[28]   C. Charalambous, "Minimax design of recursive digital filters," Computer Aided Design, vol. 6, pp. 73-81, 1974.

[29] C. Charalambous and A.R. Conn, "Optimization of microwave networks," IEEE Trans. Microwave Theory Tech., vol. MTT-23, pp. 834-838, 1975.

[30] J. Hald and K. Madsen, "Combined LP and quasi-Newton methods for minimax optimization," Math. Program., vol. 20, pp. 49-62, 1981.

[31] K. Madsen, H. Schjaer-Jacobson and J. Voldby, "Automated minimax design of networks," IEEE Trans. Circuits Syst., vol. CAS-22, pp. 791-796, 1975.

[32] M.R. Osborne and G.A. Watson, "An algorithm for minimax optimization in the nonlinear case," Comput. J., vol. 12, pp. 63-68, 1969.

[33] J.W. Bandler, S.H. Chen and K. Madsen, "An algorithm for one-sided ℓ_1 optimization with application to circuit design centering," Proc. IEEE Int. Symp. Circuits Syst. (Espoo, Finland), pp. 1795-1798, 1988.

[34] J.W. Bandler, W. Kellermann and K. Madsen, "A nonlinear ℓ_1 optimization algorithm for design, modeling and diagnosis of networks," IEEE Trans. Circuits Syst., vol. CAS-34, pp. 174-181, 1987.

[35] J. Hald and K. Madsen, "Combined LP and quasi-Newton methods for nonlinear ℓ_1 optimization," SIAM J. Numer Anal., vol. 22, pp. 68-80, 1985.

[36] M.R. Osborne and G. A. Watson, "On an algorithm for discrete nonlinear ℓ_1 optimization," Comput. J., vol. 14, pp. 184-188, 1971.

[37] J.W. Bandler, S.H. Chen and S. Daijavad, "Microwave device modeling using efficient ℓ_1 optimization: a novel approach," IEEE Trans. Microwave Theory Tech., vol. MTT-34, pp. 1282-1293, 1986.

[38] J.W. Bandler and C. Charalambous, "Practical least pth optimization of networks," IEEE Trans. Microwave Theory Tech., vol. MTT-20, pp. 834-840, 1972.

[39] J.W. Bandler, S.H. Chen, R.M. Biernacki, L. Gao, K. Madsen and H. Yu, "Huber optimization of circuits: a robust approach," IEEE Trans. Microwave Theory Tech., vol. 41, pp. 2279-2287, 1993.

[40] M.H. Bakr, J.W. Bandler and N. Georgieva, "An aggressive approach to parameter extraction," IEEE Trans. Microwave Theory Tech., vol. 47, 1999.

[41] M.H. Bakr, J.W. Bandler and N. Georgieva, "Modeling of microwave circuits exploiting space derivative mapping," IEEE MTT-S Int. Microwave Symp. Dig. (Anaheim, CA), pp. 715-718, 1999.

[42] J.W. Bandler, N. Georgieva, M.A. Ismail, J.E. Rayas-Sánchez and Q. J. Zhang, "A generalized space mapping tableau approach to device modeling," Proc. 29th European Microwave Conf. (Munich, Germany), vol. 3, pp. 231-234, 1999.

[43] J.W. Bandler, M.A. Ismail, J.E. Rayas-Sánchez and Q. J. Zhang, "Neuromodeling of microwave circuits exploiting space mapping technology," IEEE MTT-S Int. Microwave Symp. Dig. (Anaheim, CA), pp. 149-152, 1999.

[44] J.W. Bandler, M.A. Ismail, J.E. Rayas-Sánchez and Q.J. Zhang, "Neuromodeling of microwave circuits exploiting space mapping technology," IEEE Trans. Microwave Theory Tech., vol. 47, 1999.

[45] J.W. Bandler and S.H. Chen, "Circuit optimization: the state of the art," IEEE Trans. Microwave Theory Tech., vol. 36, pp. 424-443, 1988.

[46] J.W. Bandler and M.R.M. Rizk, "Optimization of electrical circuits," Math. Program. Study, vol. 11, pp. 1-64, 1979.

[47] G.C. Temes and D.Y.F. Zai, "Least pth approximation," IEEE Trans. Circuit Theory, vol. CT-16, pp. 235-237, 1969.

[48] P. Huber, Robust Statistics, Wiley, New York, 1981.

[49] H. Ekblom and K. Madsen, "Algorithms for nonlinear Huber estimation," BIT, vol. 29, pp. 60-76, 1989.

[50] C. Charalambous, "Nonlinear least pth optimization and nonlinear programming," Math. Program., vol. 12, pp. 195-225, 1977.

[51] J.W. Bandler and A.E. Salama, "Fault diagnosis of analog circuits," Proc. IEEE, vol. 73, pp. 1279-1325, 1985.

[52] J.J. Moré, "Recent developments in algorithms and software for trust region methods," in Mathematical Programming, the State of the Art, Springer Verlag, pp. 258-287, 1982.

[53] K. Madsen, "An algorithm for minimax solution of overdetermined systems of non-linear equations," J. Inst. Math. Appl., vol. 16, pp. 321-328, 1975.

[54] K. Madsen and H. Schjær-Jacobsen, "Singularities in minimax optimization of networks," IEEE Trans. Circuits and Syst, vol. CAS-23, pp. 456-460, 1976.

[55] J.W. Bandler, "Optimization of design tolerances using nonlinear programming," J. Optimization Theory and Applications, vol. 14, pp. 99-114, 1974.

[56] J.W. Bandler, P.C. Liu and H. Tromp, "A nonlinear programming approach to optimal design centering, tolerancing and tuning," IEEE Trans. Circuits Syst., vol. CAS-23, pp. 155-165, 1976.

[57] J.W. Bandler and H.L. Abdel-Malek, "Optimal centering, tolerancing and yield determination via updated approximations and cuts," IEEE Trans. Circuits Syst., vol. CAS-25, pp. 853-871, 1978.

[58] H.L. Abdel-Malek and J.W. Bandler, "Yield optimization for arbitrary statistical distributions, Part I: Theory," IEEE Trans. Circuits Syst., vol. CAS-27, pp. 245-253, 1980.

[59] H.L. Abdel-Malek and J.W. Bandler, "Yield optimization for arbitrary statistical distributions, Part II: Implementation," IEEE Trans. Circuits Syst., vol. CAS-27, pp. 253-262, 1980.

[60]   J.W. Bandler, R.M. Biernacki, S.H. Chen, S. Ye and P.A. Grobelny, "Multilevel multidimensional quadratic modeling for yield-driven electromagnetic optimization," IEEE MTT-S Int. Microwave Symp. Dig. (Atlanta, GA), pp. 1017-1020, 1993.

[61]   S. Bila, D. Baillargeat, S. Verdeyme and P. Guillon, "Automated design of microwave devices using full em optimization method," IEEE MTT-S Int. Microwave Symp. Dig. (Baltimore, MD), pp. 1771-1774, 1998.

[62]   A.M. Pavio, "The electromagnetic optimization of microwave circuits using companion models," Proc. Workshop on Novel Methodologies for Device Modeling and Circuit CAD, IEEE MTT-S Int. Microwave Symp. (Anaheim, CA), 1999.

[63]   M.H. Bakr, J.W. Bandler, R.M. Biernacki and S.H. Chen, "Design of a three-section 3:1 microstrip transformer using aggressive space mapping," Report SOS-97-1-R, Simulation Optimization Systems Research Laboratory, McMaster University, Hamilton, Canada, 1997.

[64]   *em*™ , Sonnet Software, Inc., 1020 Seventh North Street, Suite 210, Liverpool, NY 13088, 1997.

[65]   OSA90/hope™ Version 4.0, formerly Optimization Systems Associates Inc., P.O. Box 8083, Dundas, ON, Canada, L9H 5E7, 1997, now HP EEsof Division, 1400 Fountaingrove Parkway, Santa Rosa, CA 95403-1799.

[66]   K. Levenberg, "A method for the solution of certain problems in least squares," Quart. Appl. Math., vol. 2, pp. 164-168, 1944.

[67]   D. Marquardt, "An algorithm for least-squares estimation of non-linear parameters," SIAM J. Appl. Math., vol. 11, pp. 431-441, 1963.

[68]   J.J. Moré and D.C. Sorenson, "Computing a trust region step," SIAM J. Sci. Stat. Comp., vol. 4, pp. 553-572, 1983.

[69]   L. Young and B.M. Schiffman, "A useful high-pass filter design," Microwave J., vol. 6, pp. 78-80, 1963.

[70]   G.L. Matthaei, L. Young and E.M. T. Jones, Microwave Filters, Impedance-Matching Network and Coupling Structures, McGraw-Hill, New York, First Edition, 1964.

[71]   HP HFSS™ Version 5.2, Agilent Technologies, 1400 Fountaingrove Parkway, Santa Rosa, CA 95403-1799, 1998.

[72]   HP Empipe3D™ Version 5.2, Agilent Technologies, 1400 Fountaingrove Parkway, Santa Rosa, CA 95403-1799, 1998.

[73]   N. Marcuvitz, Waveguide Handbook, McGraw-Hill, New York, First Edition, p. 221, 1951.

[74]   J.W. Bandler, R.M. Biernacki, S.H. Chen and Q.H. Wang, "Multiple space mapping EM optimization of signal integrity in high-speed digital circuits," Proc. 5th Int. Workshop on Integrated Nonlinear Microwave and Millimeterwave Circuits (Duisburg, Germany), pp. 138-140, 1998.

[75]   P. Burrascano and M. Mongiardo, "A review of artificial neural networks applications in microwave CAD," Int. J. RF and Microwave CAE, Special Issue on Applications of ANN to RF and Microwave Design, vol. 9, pp. 158-174, 1999.

[76]   A.H. Zaabab, Q.J. Zhang and M.S. Nakhla, "A neural network modeling approach to circuit optimization and statistical design," IEEE Trans. Microwave Theory Tech., vol. 43, pp. 1349-1358, 1995.

[77]   P. Watson and K.C. Gupta, "EM-ANN models for microstrip vias and interconnects in multilayer circuits," IEEE Trans. Microwave Theory Tech., vol. 44, pp. 2495-2503, 1996.

[78]   M.H. Bakr, J.W. Bandler, M.A. Ismail, J.E. Rayas-Sánchez and Q.J. Zhang, "Neural frequency-space mapping optimization of EM microwave structures," IEEE MTT-S Int. Microwave Symp. Digest (Boston, MA), pp. 879-882, 2000.

[79]   A.J. Booker, J.E. Dennis, Jr., P.D. Frank, D. B. Serafini, V. Torczon and M.W. Trosset, "A rigorous framework for optimization of expensive functions by surrogates," Structural Optimization, vol. 17, pp. 1-13, 1999.

[80]   M.W. Trosset and V, Torczon, "Numerical optimization using computer experiments," Technical Report 97-38, ICASE, NASA Langley Research Center, Hampton, Virginia 23681-2199, 1997.

[81]   V. Torczon and M.W. Trosset, "Using approximations to accelerate engineering design optimization," Technical Report 98-33, ICASE, Langley Research Center, Hampton, Virginia 23681-2199, 1998.

[82]   J.E. Dennis, Jr., and V. Torczon, "Managing approximation models in optimization," Technical Report 95-19, Department of Computational and Applied Mathematics, Rice University, Houston, Texas 77005-1892, 1995.

[83]   N. Alexandrov, J.E. Dennis, Jr., R.M. Lewis and V. Torczon, "A trust region framework for managing the use of approximation models in optimization," Structural Optimization, vol. 15, pp. 16-23, 1998.

[84]   M.H. Bakr, J.W. Bandler, K. Madsen, J.E. Rayas-Sánchez and J. Søndergaard, "Space mapping optimization of microwave circuits exploiting surrogate models," IEEE MTT-S Int. Microwave Symp. Dig. (Boston, MA), pp. 1785-1788, 2000.

(a)

(b)

(c)
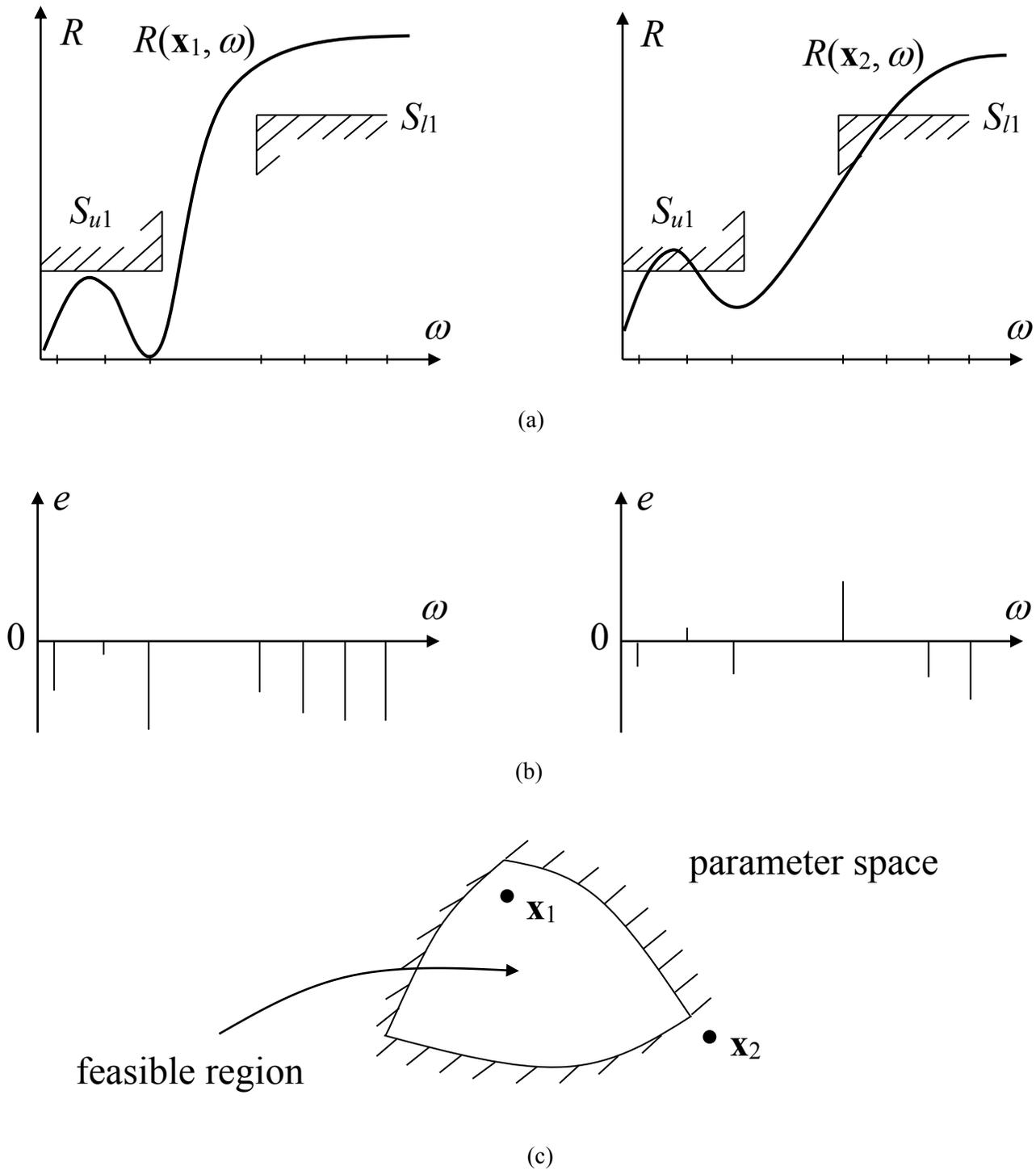
Fig. 1. Illustration of some basic engineering optimization concepts; (a) the responses at a feasible design $\mathbf{x}_1$ and an infeasible design $\mathbf{x}_2$, (b) the error functions at sampled values of the independent parameter ω and (c) a possible location of the two designs with respect to the feasible region for a two-dimensional case.

parameter space

feasible region

yield=1

yield=0

0<yield<1

Δx_2

Δx_1
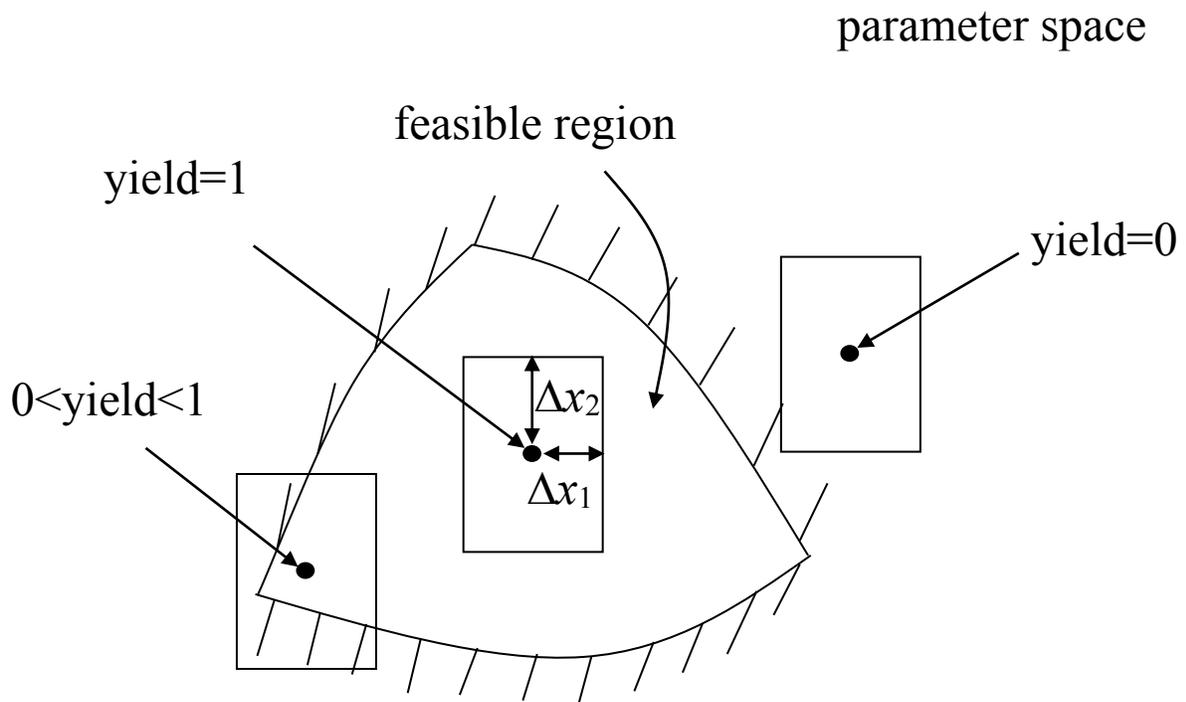
Fig. 2.   Illustration of design centering and yield for a two-dimensional problem with manufacturing tolerances of Δx_1 and Δx_2.   Three different designs are shown; a centered design where all possible outcomes are feasible (yield=1), an infeasible design where possible outcomes are infeasible (yield=0) and non centered feasible design where possible outcomes may be feasible or infeasible (0<yield<1).

$$\mathbf{R}_c(\mathbf{x}_c^{(i)}) \approx \mathbf{R}_f(\mathbf{x}_f^{(i)})$$
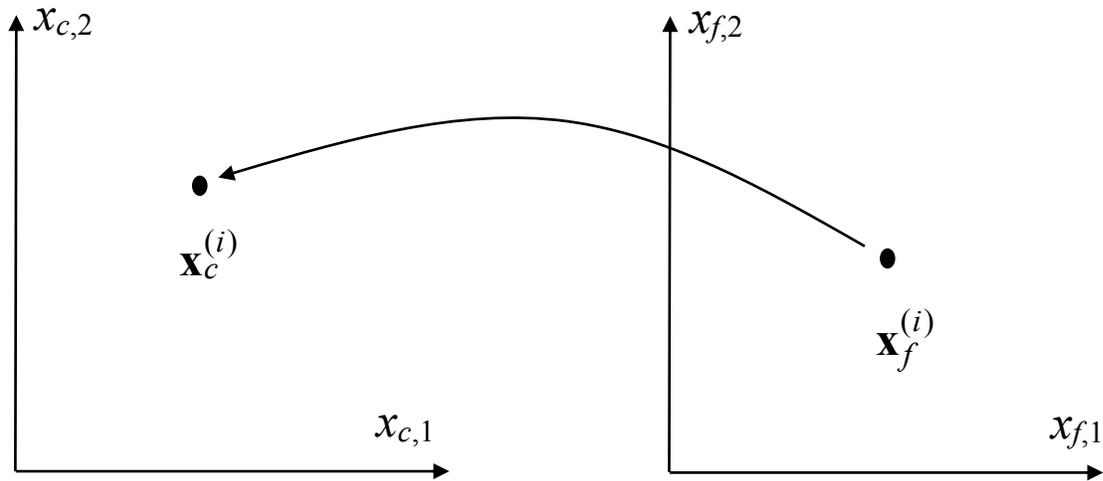
Fig. 3. Illustration of the SPE procedure for a two-dimensional problem.
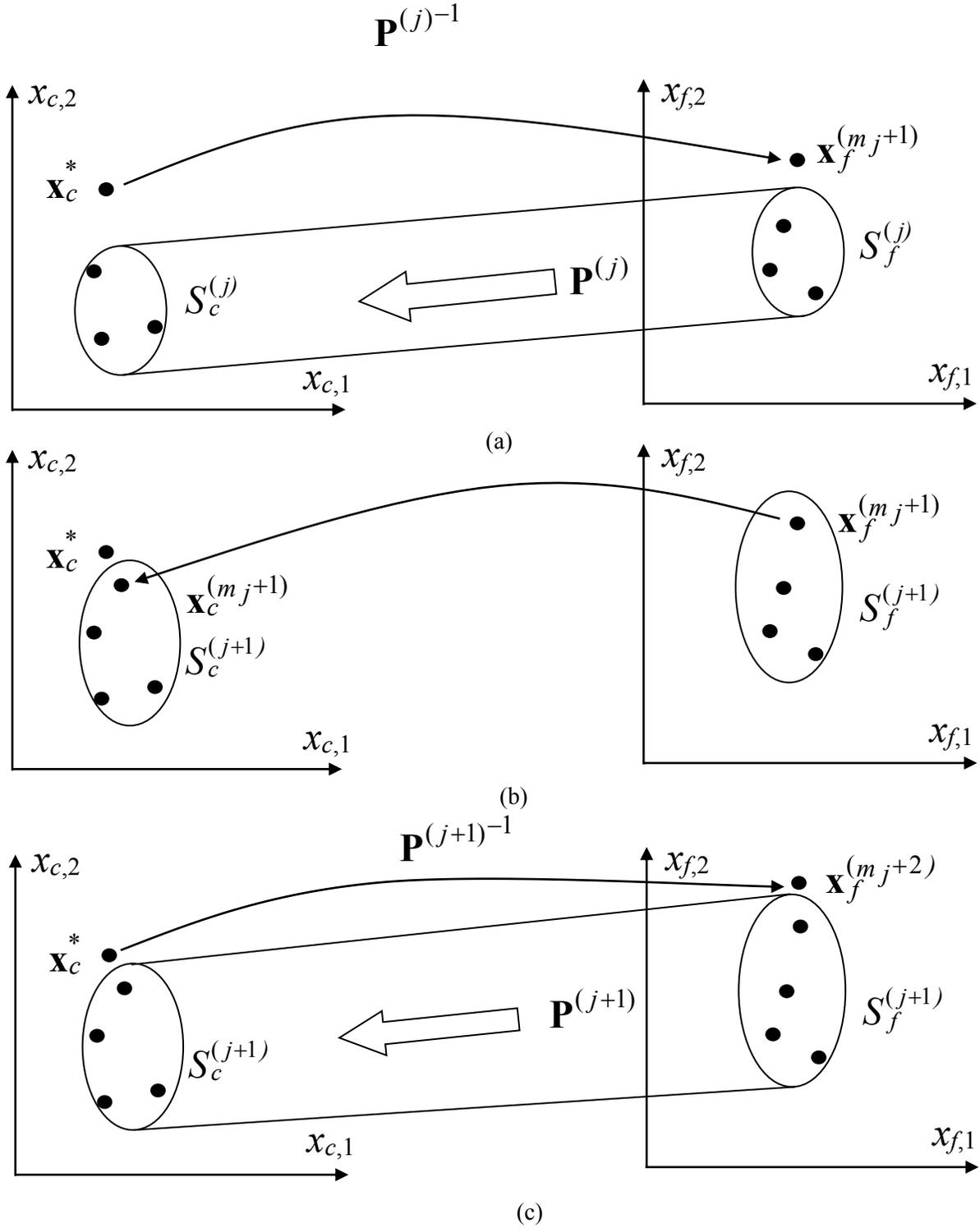
Fig. 4. Illustration of the original SM optimization algorithm; (a) a new point $\mathbf{x}_f^{(m_j+1)}$ is obtained using the current mapping approximation $\mathbf{P}^{(j)}$, (b) the point $\mathbf{x}_f^{(m_j+1)}$ does not satisfy the stopping criterion and the sets $S_f^{(j)}$ and $S_c^{(j)}$ are augmented by $\mathbf{x}_f^{(m_j+1)}$ and $\mathbf{x}_c^{(m_j+1)}$, respectively, and (c) a new mapping $\mathbf{P}^{(j+1)}$ is estimated and is used to obtain a new iterate $\mathbf{x}_f^{(m_j+2)}$.

$$\mathbf{B}^{(j)}\mathbf{h}^{(j)} = -\mathbf{f}^{(j)}$$

(a)

(b)

$$\mathbf{B}^{(j+1)}\mathbf{h}^{(j+1)} = -\mathbf{f}^{(j+1)}$$

(c)
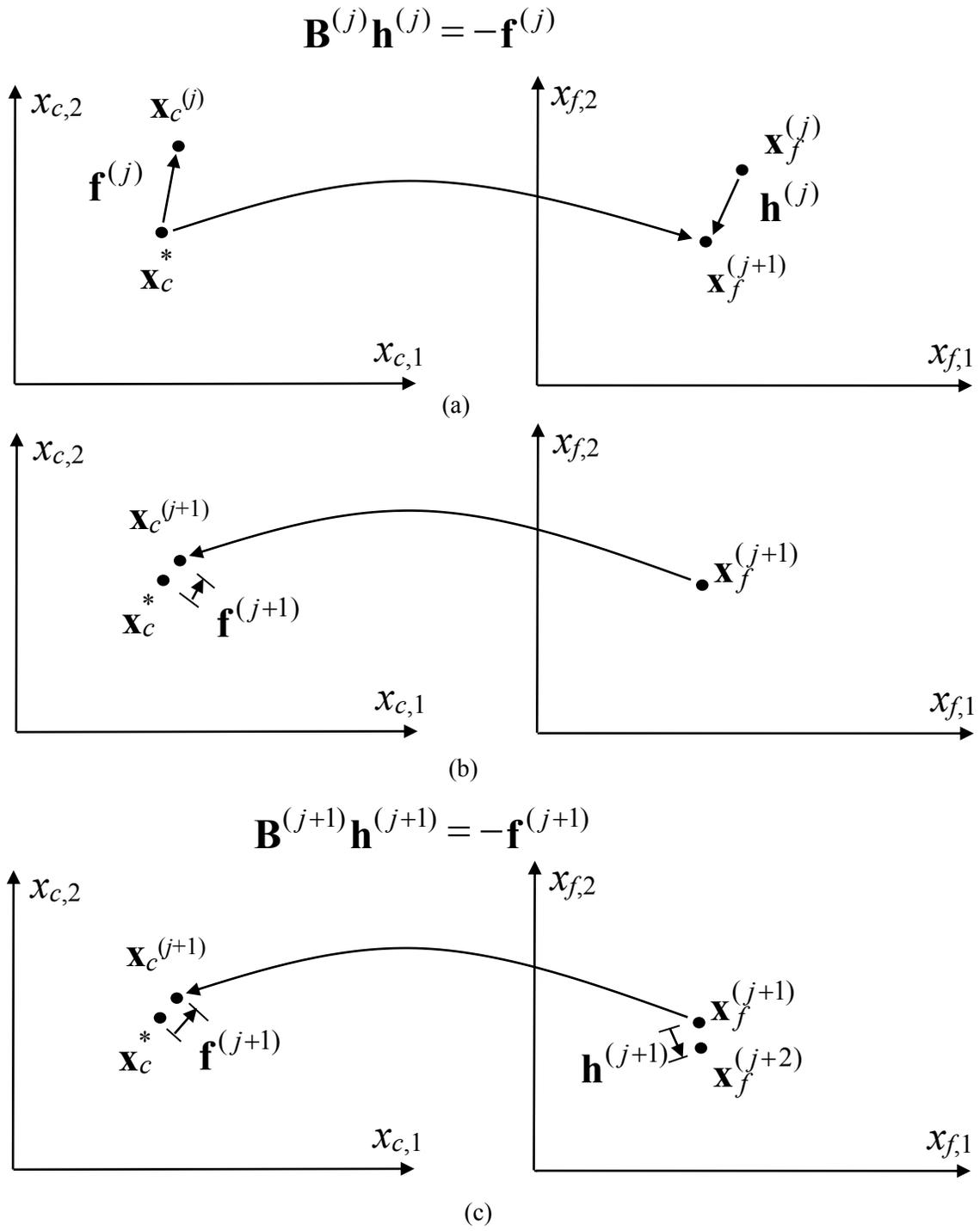
Fig. 5. Illustration of ASM; (a) a new iterate $\mathbf{x}_f^{(j+1)}$ is obtained, (b) by applying parameter extraction we find that the stopping criterion is not satisfied ($\left\|\mathbf{f}^{(j+1)}\right\| > \varepsilon$) and (c) the updated matrix $\mathbf{B}^{(j+1)}$ is used to predict a new iterate $\mathbf{x}_f^{(j+2)}$.
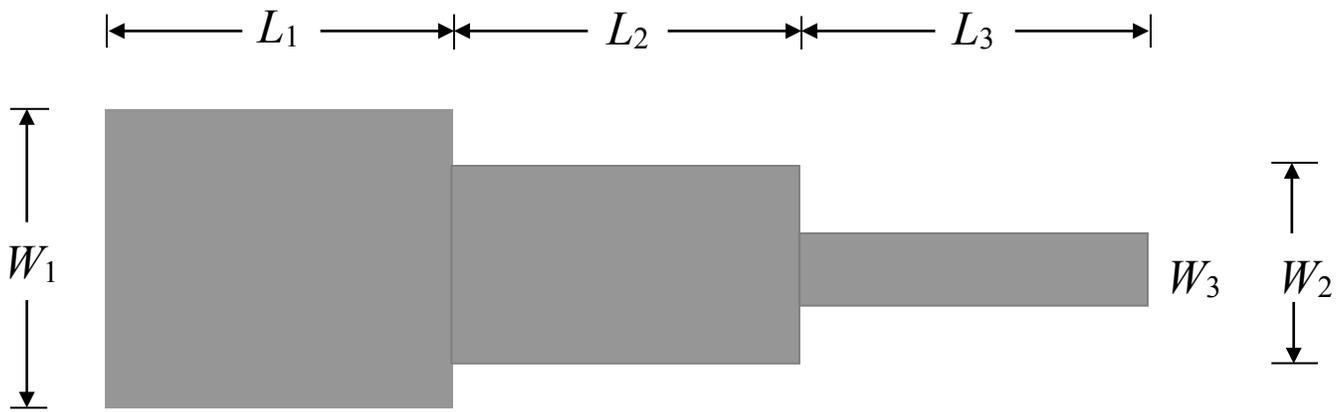
Fig. 6. The three-section 3:1 microstrip impedance transformer [63].
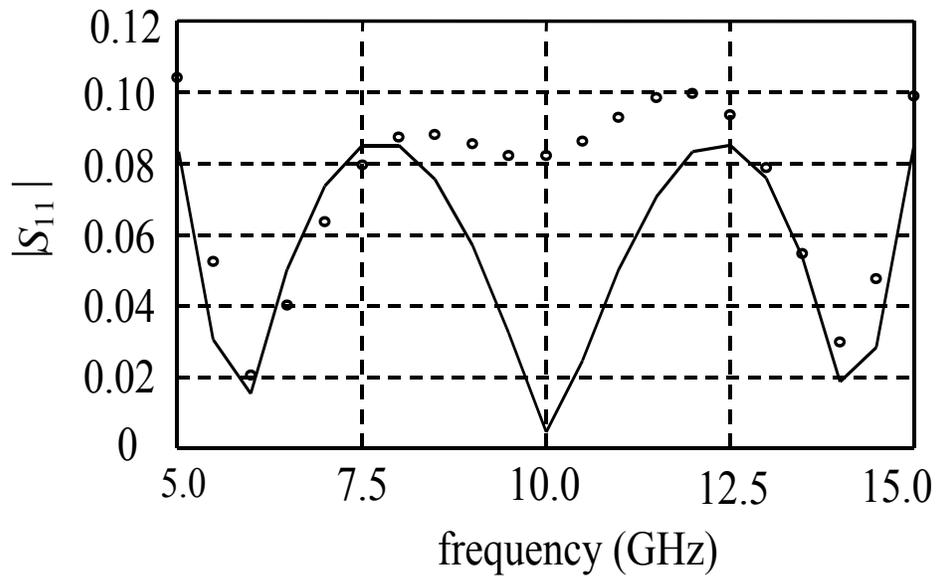
Fig. 7. The optimal coarse model response (—) and the fine model response (o) at the initial design for the three-section microstrip transformer.
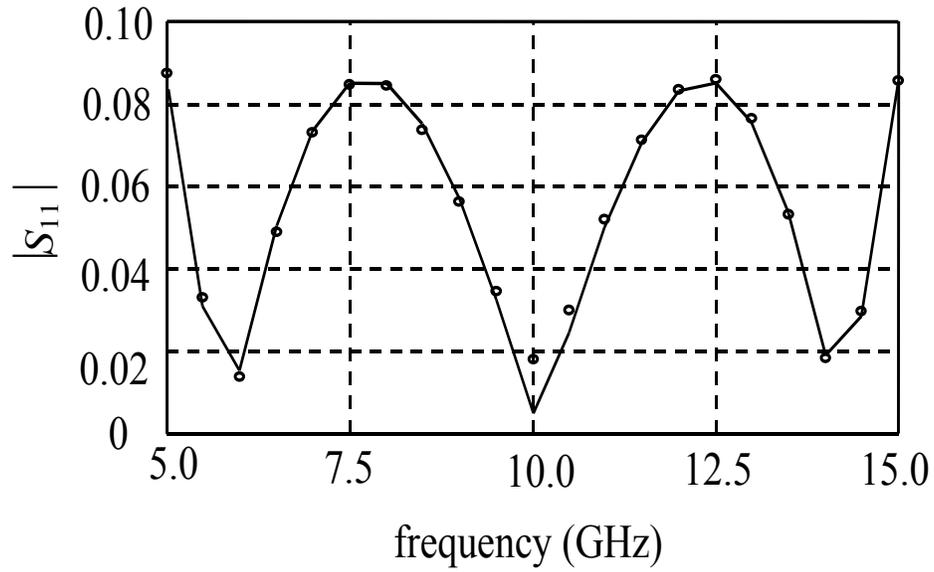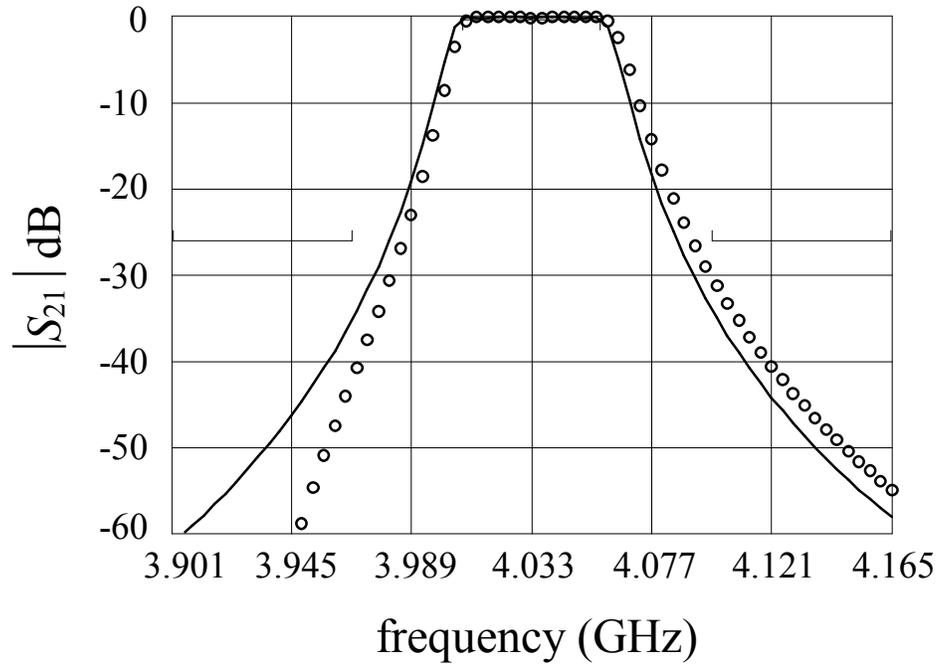
Fig. 8. The optimal coarse model response (—) and the fine model response (o) at the space-mapped design for the three-section microstrip transformer.
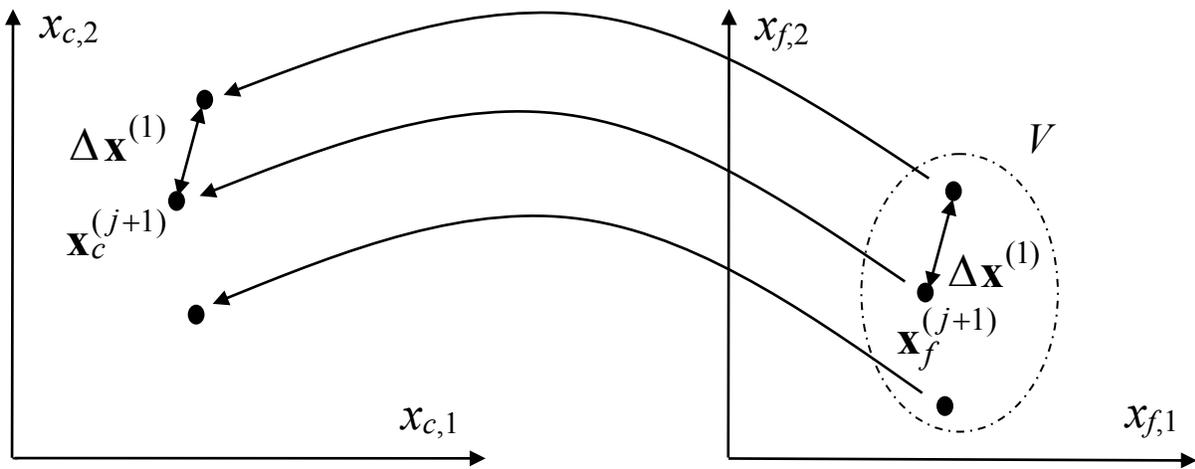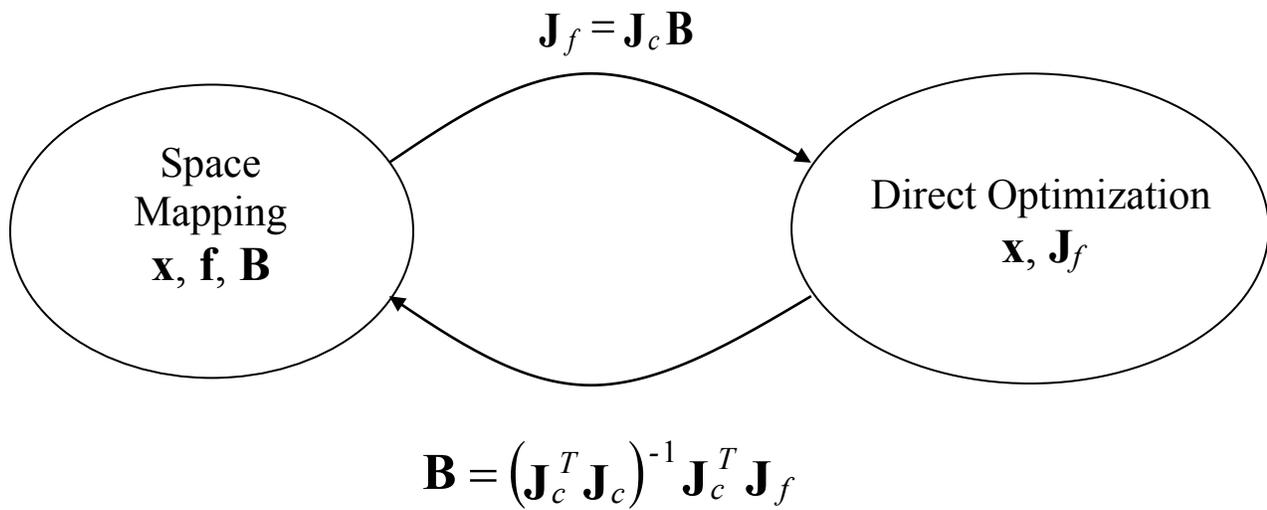

Fig. 9. Illustration of MPE at the jth iteration.
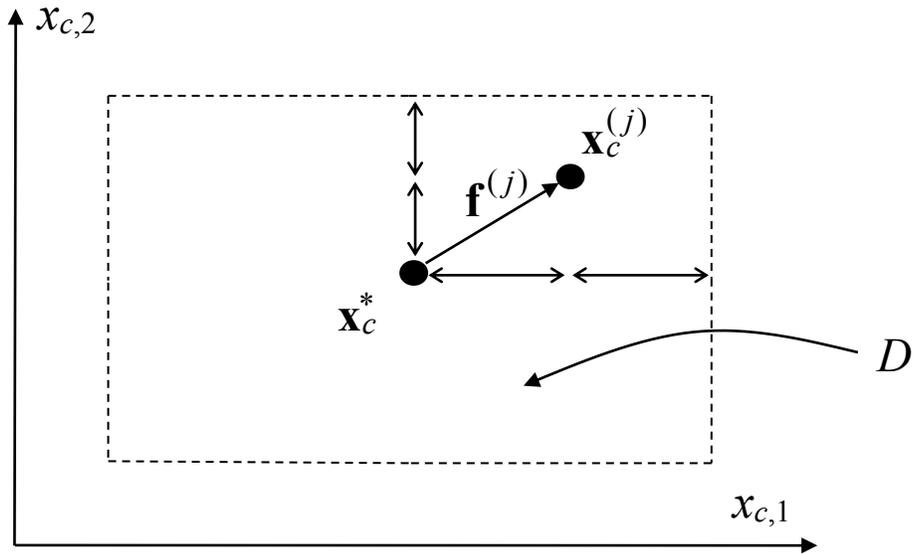
Fig. 10. The region utilized in the statistical parameter extraction approach for obtaining $\mathbf{x}_c^*$.
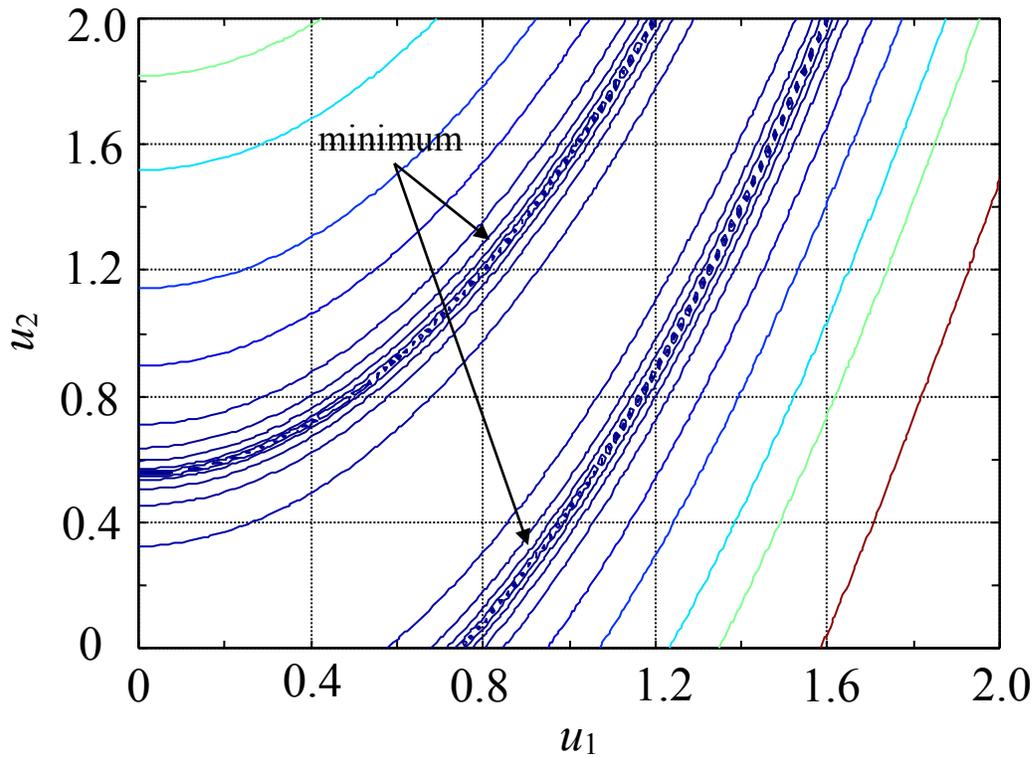
Fig. 11. Illustration of a locally nonunique solution of parameter extraction for a two-dimensional case.
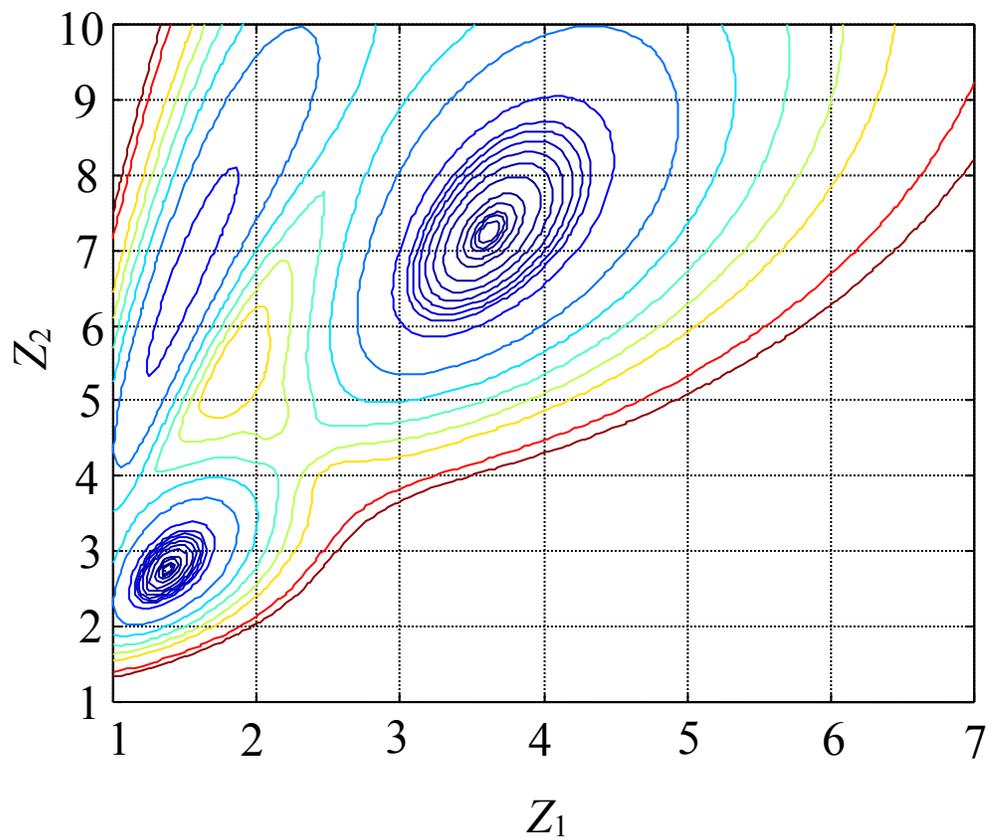
Fig. 12.   Illustration of a locally unique solution of parameter extraction for a two-dimensional case; three locally unique minima are shown.
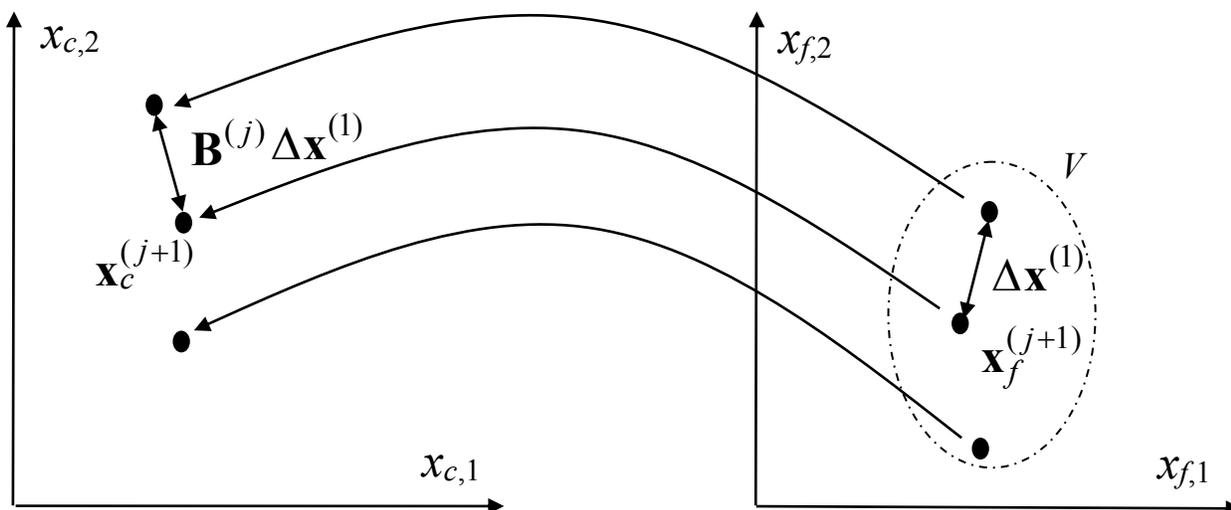
Fig. 13. Illustration of RMPE.
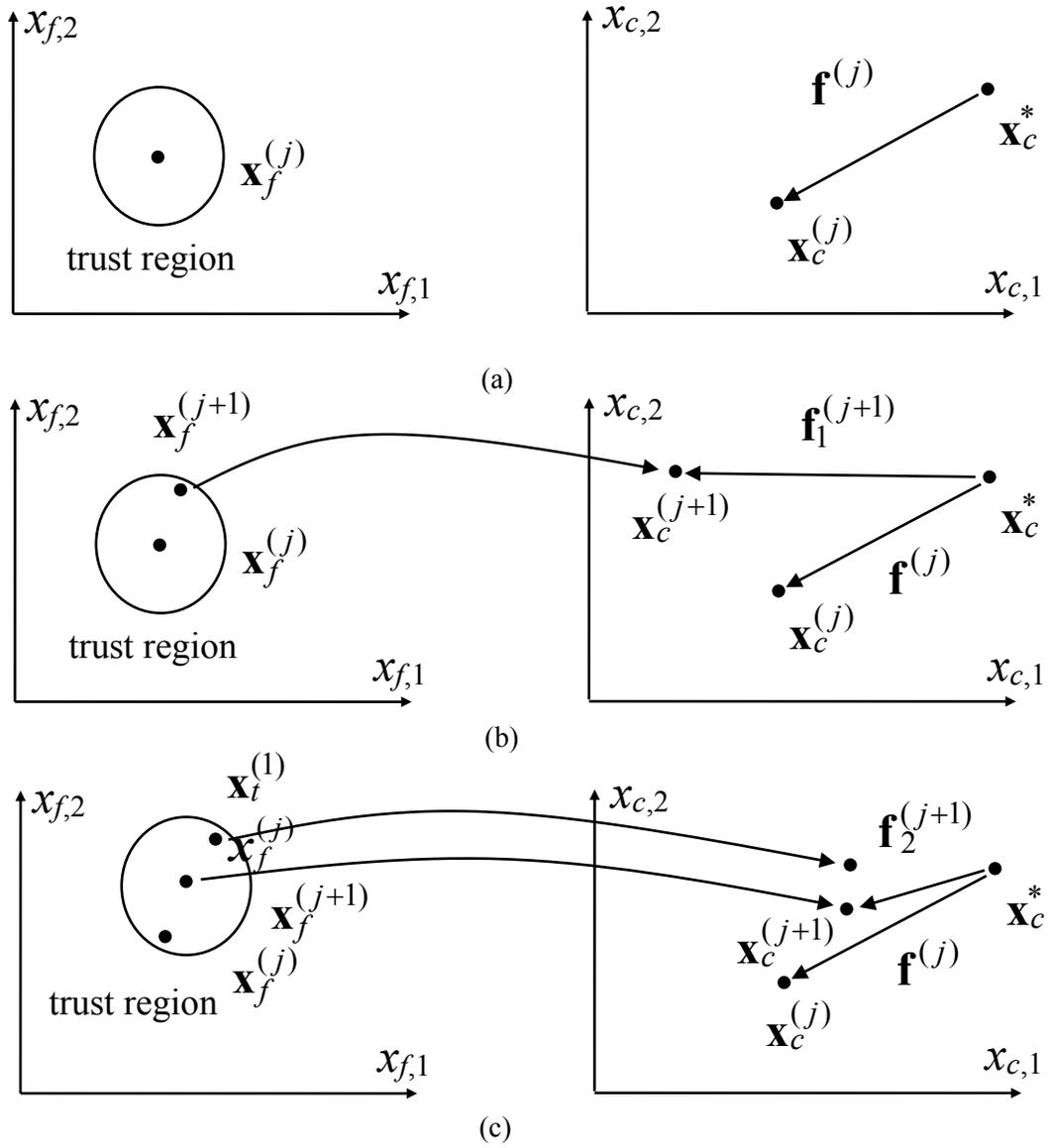
Fig. 14. Illustration of the TRASM algorithm; (a) in the jth iteration the point $\mathbf{x}_f^{(j)}$ corresponds to a trusted error vector $\mathbf{f}^{(j)}$, (b) a new iterate $\mathbf{x}_f^{(j+1)}$ is taken and SPE is carried out to get $\mathbf{f}_1^{(j+1)}$ and (c) the vector $\mathbf{f}_1^{(j+1)}$ does not satisfy the success criterion so a temporary point $\mathbf{x}_t^{(1)}$ is generated and two-point extraction is carried out to get $\mathbf{f}_2^{(j+1)}$ which satisfies the success criterion.
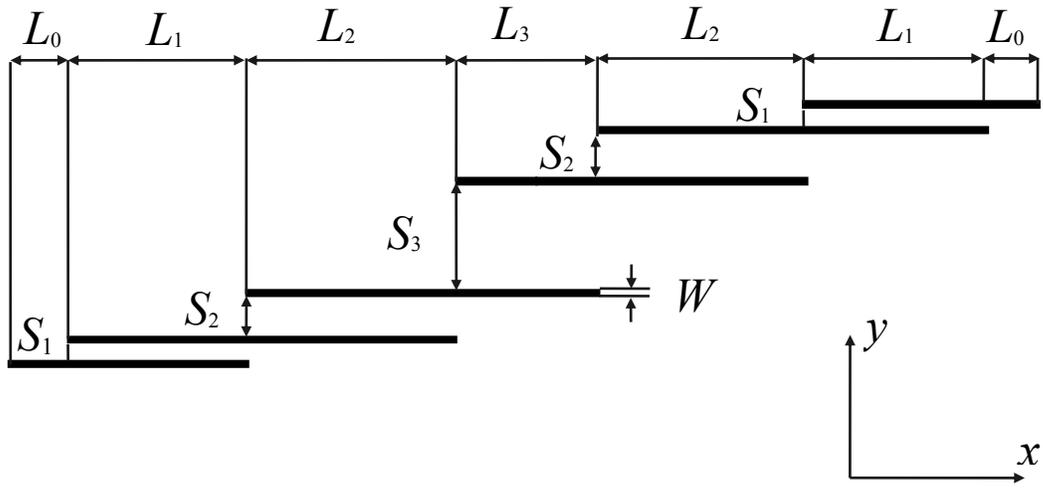
Fig. 15. The structure of the HTS filter [1].
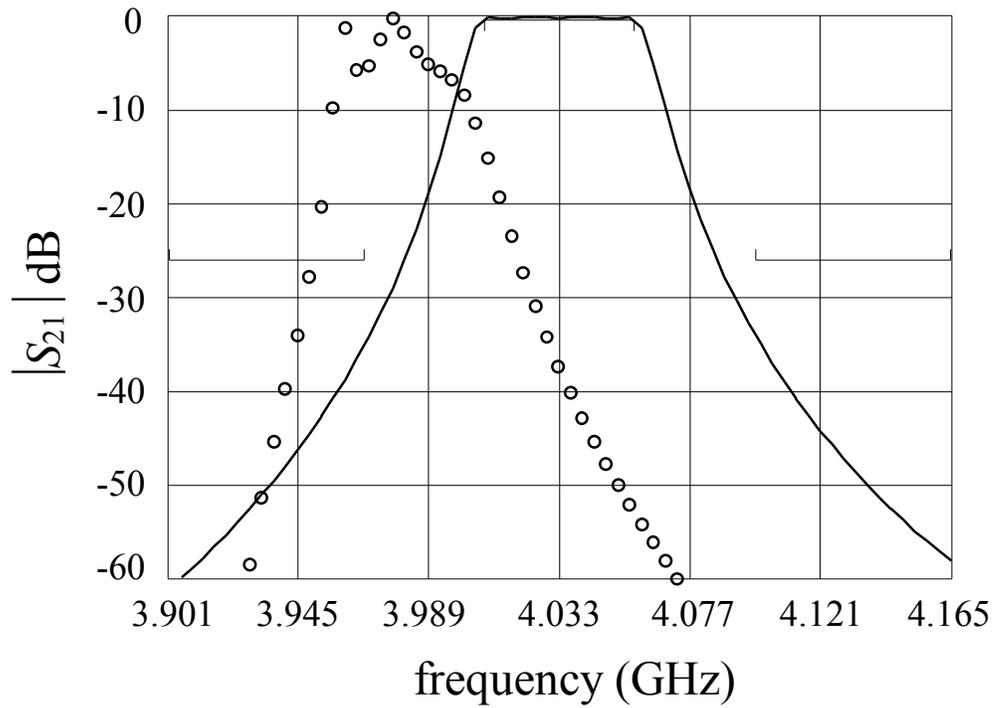
Fig. 16. The optimal coarse model response (—) and the fine model response (○) at the initial design for the HTS filter.

Fig. 17. The optimal coarse model response (—) and the fine model response (o) at the space-mapped design for the HTS filter.

$$\mathbf{J}_f = \mathbf{J}_c \mathbf{B}$$

Space Mapping
$\mathbf{x}, \mathbf{f}, \mathbf{B}$

Direct Optimization
$\mathbf{x}, \mathbf{J}_f$

$$\mathbf{B} = \left(\mathbf{J}_c^T \mathbf{J}_c\right)^{-1} \mathbf{J}_c^T \mathbf{J}_f$$

Fig. 18. Illustration of the connection between SM optimization and direct optimization.

46
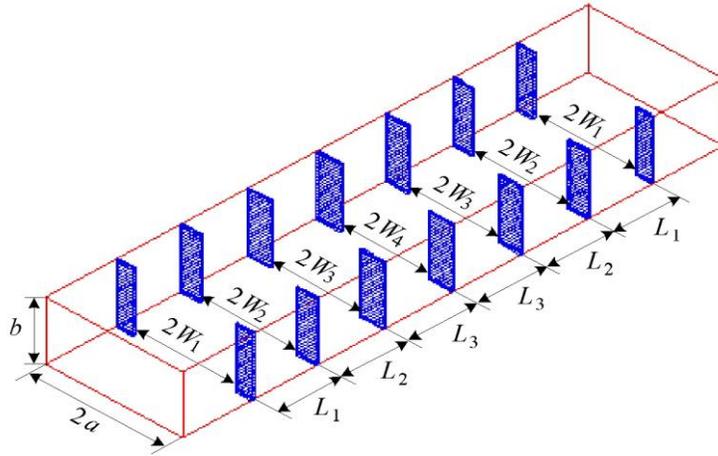
Fig. 19. The fine model of the six-section H-plane waveguide filter [69, 70].
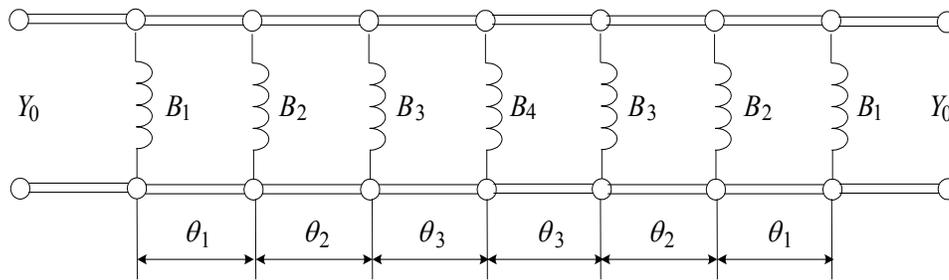
Fig. 20. The coarse model of the six-section H-plane waveguide filter [73].
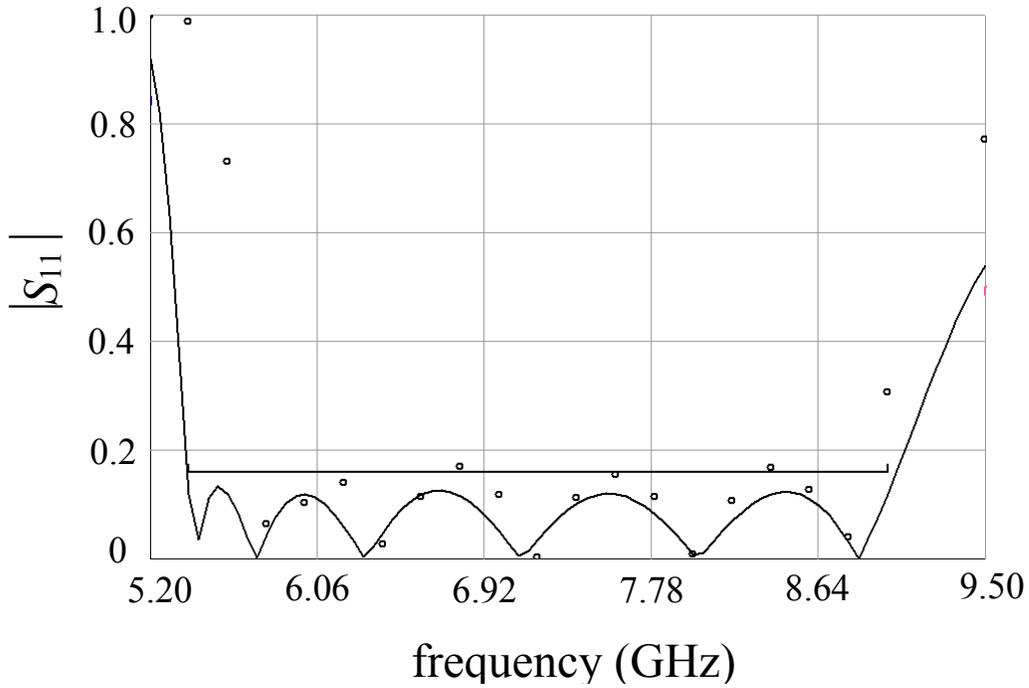
Fig. 21. The optimal coarse response (—) and the fine response (o) at the initial design for the six-section H-plane waveguide filter.
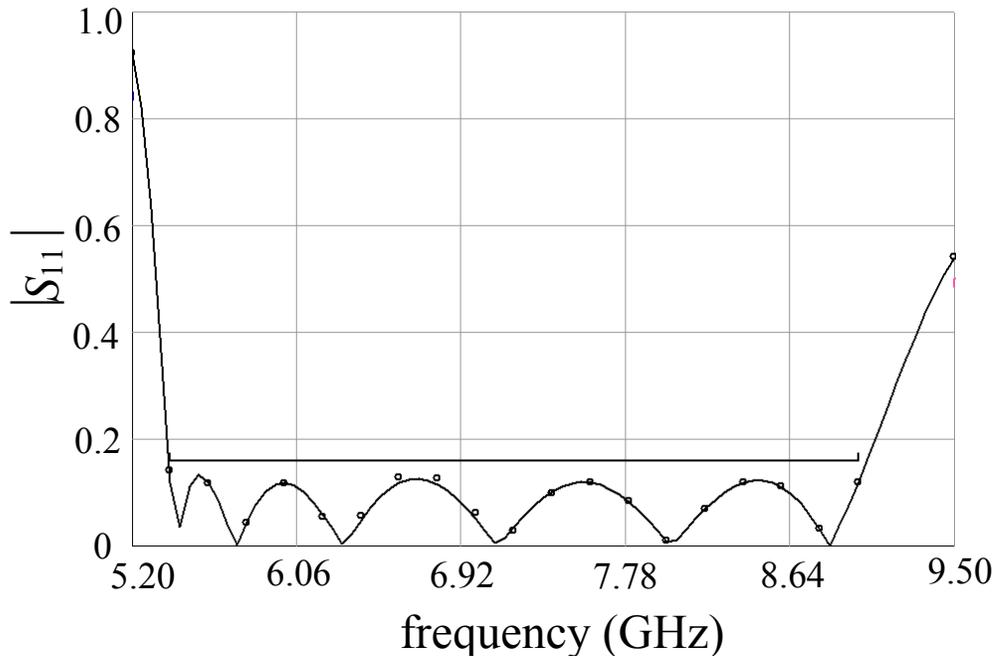
Fig. 22. The optimal coarse response (—) and the fine response (o) at the end of the second phase for the six-section H-plane waveguide filter.
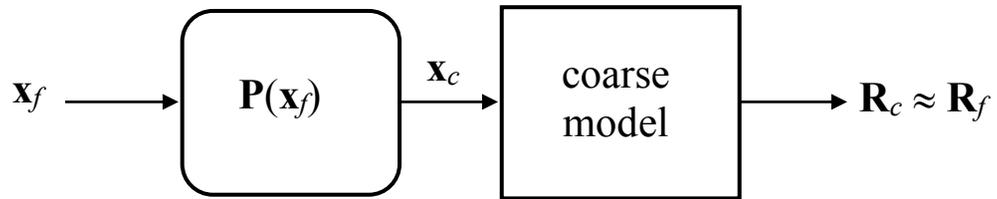
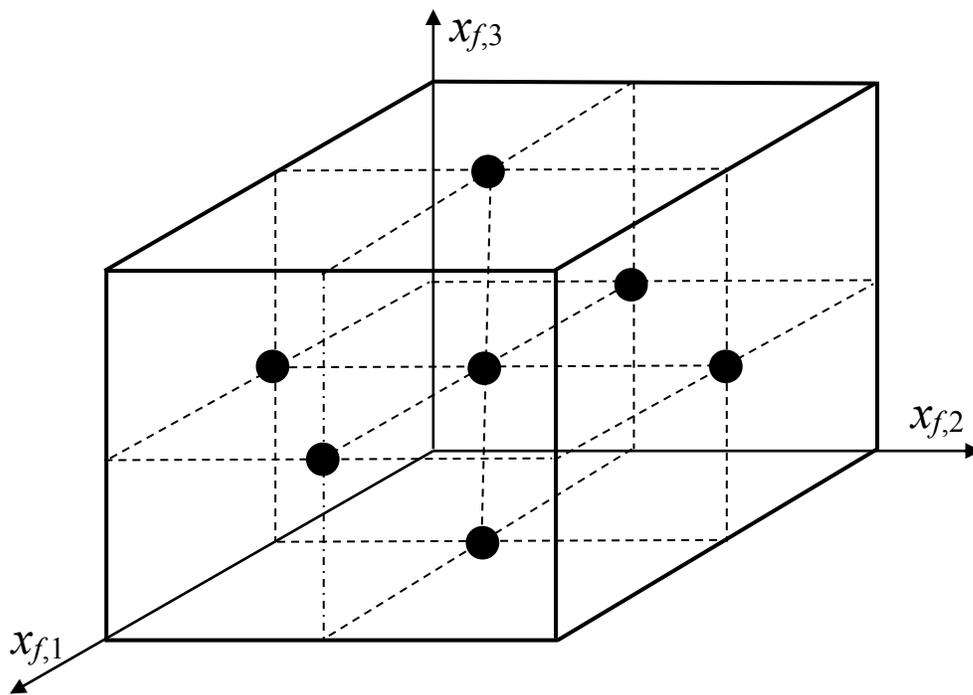Fig. 23. Illustration of the SM approach to engineering modeling.

Fig. 24. A three-dimensional illustration of the star distribution utilized in GSM and SMN.
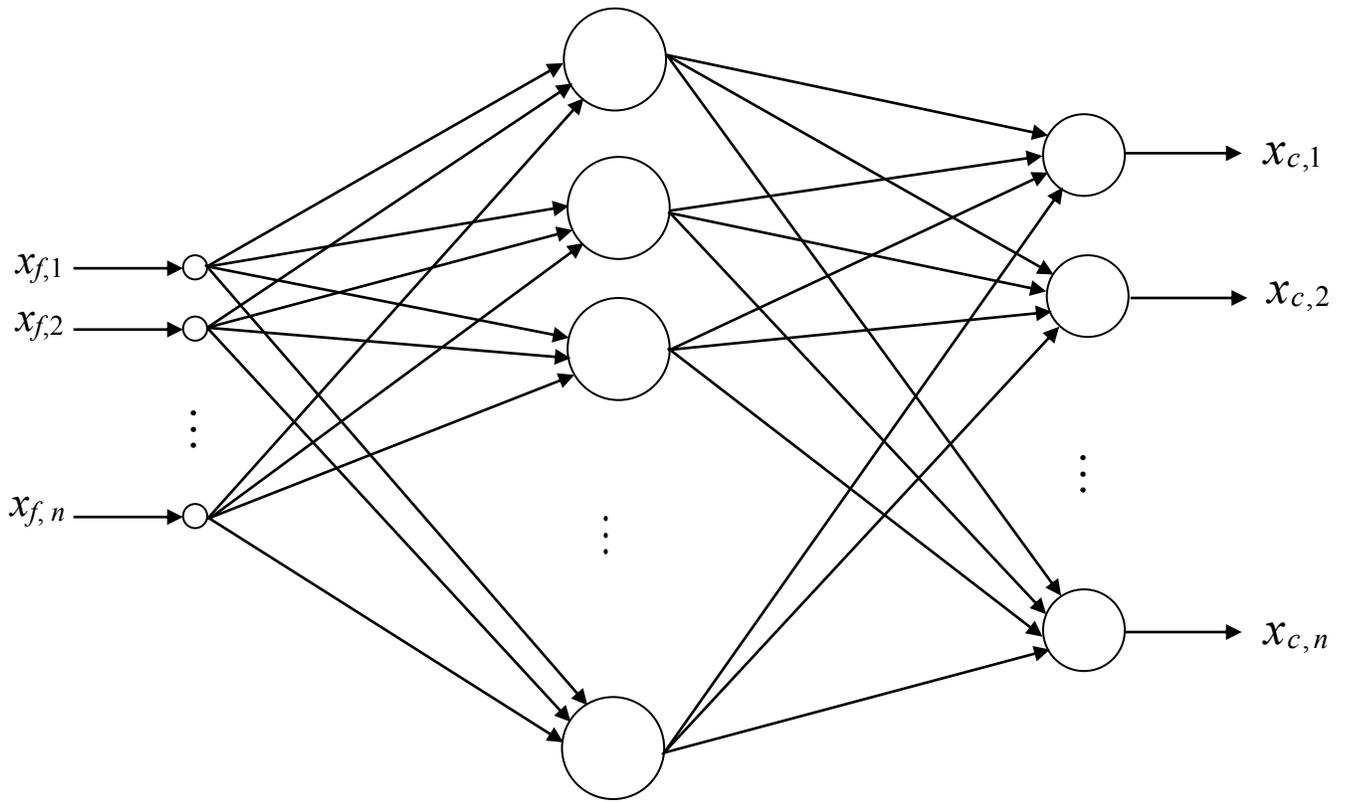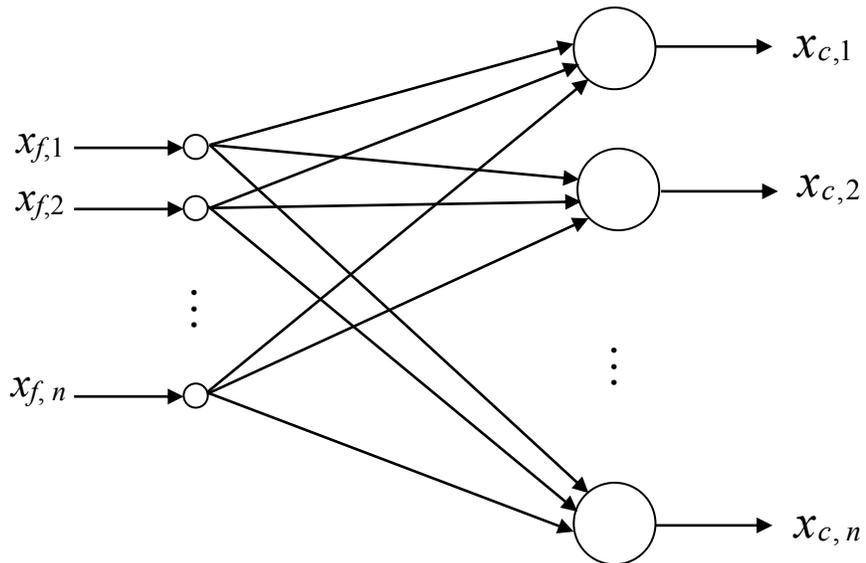
Fig. 25. Illustration of the SMN approach.

Fig. 26. Illustration of GSM as a special case of SMN.